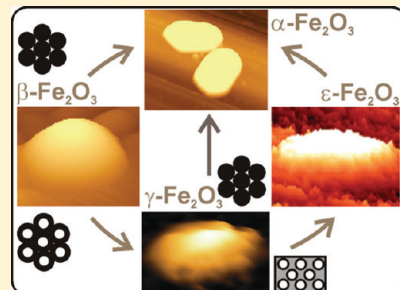


Polymorphous Transformations of Nanometric Iron(III) Oxide: A Review

Libor Machala, Jiří Tuček, and Radek Zbořil*

Regional Centre of Advanced Technologies and Materials, Departments of Physical Chemistry and Experimental Physics, Faculty of Science, Palacky University, Slechtitelu 11, 783 71 Olomouc, Czech Republic

ABSTRACT: There is great interest in iron oxides, especially in nanosized form, for both fundamental and practical reasons. Because of its polymorphism, iron(III) oxide (ferric oxide, Fe_2O_3) is one of the most interesting and potentially useful phases of the iron oxides. Each of the four different known crystalline Fe_2O_3 polymorphs (alpha-, beta-, gamma-, and epsilon- Fe_2O_3) has unique biochemical, magnetic, catalytic, and other properties that make it suitable for specific technical and biomedical applications. High temperature treatment is a key step in most syntheses of iron(III) oxides but often triggers polymorphous transformations that result in the formation of undesired mixtures of Fe_2O_3 polymorphs. It is therefore important to control the parameters that induce polymorphous transformations when seeking to prepare a given Fe_2O_3 polymorph as a single phase; identifying and understanding these parameters is a major challenge in the study of the polymorphism of solid compounds. This review discusses the dependence of the mechanism and kinetics of the polymorphous transformations of Fe_2O_3 on the intrinsic properties of the material (polymorph structure, particle size, particle morphology, surface coating, particle aggregation, incorporation of particles within a matrix) and external parameters of synthetic and/or natural conditions such as temperature, atmosphere, and pressure. The high-temperature and high-pressure induced transformations of Fe_2O_3 are reviewed in detail. In addition, the question of whether different Fe_2O_3 polymorphs are formed sequentially or simultaneously during thermal processes is discussed extensively, with reference to the experimental results that have been invoked to support these two different mechanisms. The use of selected analytical tools in studying the polymorphous transformations of Fe_2O_3 is also discussed, with particular emphasis on in situ approaches. Finally, key objectives for future research in this area are highlighted: (i) the development of more sophisticated kinetic control of the $\gamma\text{-}\text{Fe}_2\text{O}_3 \rightarrow \varepsilon\text{-}\text{Fe}_2\text{O}_3$ phase transformation; (ii) investigation of particle morphology changes during the polymorphous transformations of Fe_2O_3 ; and (iii) the study of high-pressure induced phase transformations of Fe_2O_3 polymorphs other than $\alpha\text{-}\text{Fe}_2\text{O}_3$.



KEYWORDS: polymorphous transformations, maghemite, hematite, nanoparticle, $\beta\text{-}\text{Fe}_2\text{O}_3$, $\varepsilon\text{-}\text{Fe}_2\text{O}_3$

1. INTRODUCTION

To date, four crystalline polymorphs of Fe_2O_3 (also known as iron(III) oxide or ferric oxide) have been described, all of which have significantly different structural and magnetic properties: (i) $\alpha\text{-}\text{Fe}_2\text{O}_3$; (ii) $\beta\text{-}\text{Fe}_2\text{O}_3$; (iii) $\gamma\text{-}\text{Fe}_2\text{O}_3$; and (iv) $\varepsilon\text{-}\text{Fe}_2\text{O}_3$.^{1–3} Moreover, it has been observed that exposure of $\alpha\text{-}\text{Fe}_2\text{O}_3$ to extremely high pressures results in the formation of a new perovskite-type “high-pressure Fe_2O_3 structure”.^{5–9} While the highly crystalline $\alpha\text{-}\text{Fe}_2\text{O}_3$ and $\gamma\text{-}\text{Fe}_2\text{O}_3$ occur in nature, $\beta\text{-}\text{Fe}_2\text{O}_3$ and $\varepsilon\text{-}\text{Fe}_2\text{O}_3$ are generally synthesized in the laboratory, as are nanoparticles of the different structural forms.⁴ In addition to the crystalline forms, it is also possible to prepare amorphous Fe_2O_3 , the properties of which have attracted much interest in recent years.^{10–13} In amorphous Fe_2O_3 , the Fe(III) ions are surrounded by oxygen octahedra whose symmetry axes are randomly orientated in a nonperiodic lattice. All of the crystalline polymorphs can generally be synthesized as powders, thin films, composites, or coated particles.

The principal aim of this short critical review is to discuss mechanisms and kinetics of polymorphous transitions of iron(III) oxide under various conditions and with respect to the form of Fe_2O_3 specimen. Particular emphasis is placed upon thermally

induced polymorphous transitions, which often occur during the synthesis and use of Fe_2O_3 . The potential impact of the simultaneous formation of two ferric oxide polymorphs on these transformation mechanisms is addressed in detail. In addition, some of the experimental tools used to study the polymorphous transformations of Fe_2O_3 are discussed, with a particular emphasis on in situ approaches. Finally, various methodological issues (including the use of isothermal and dynamic heating) and the issue of distinguishing between nanocrystalline and amorphous Fe_2O_3 are considered.

Surprisingly, this is the first published attempt at summarizing all of the possible polymorphous transformations of iron(III) oxide. This review complements those previously published by our group^{2,3,10,14} and draws on our extensive experience with the synthesis, characterization, and applications of iron(III) oxide nanoparticles.

1.1. $\alpha\text{-}\text{Fe}_2\text{O}_3$. $\alpha\text{-}\text{Fe}_2\text{O}_3$ (mineralogically known as hematite) has a rhombohedrally centered hexagonal structure of the corundum type with a close-packed oxygen lattice in which two-thirds of the

Received: February 8, 2011

Revised: May 9, 2011

Published: June 01, 2011

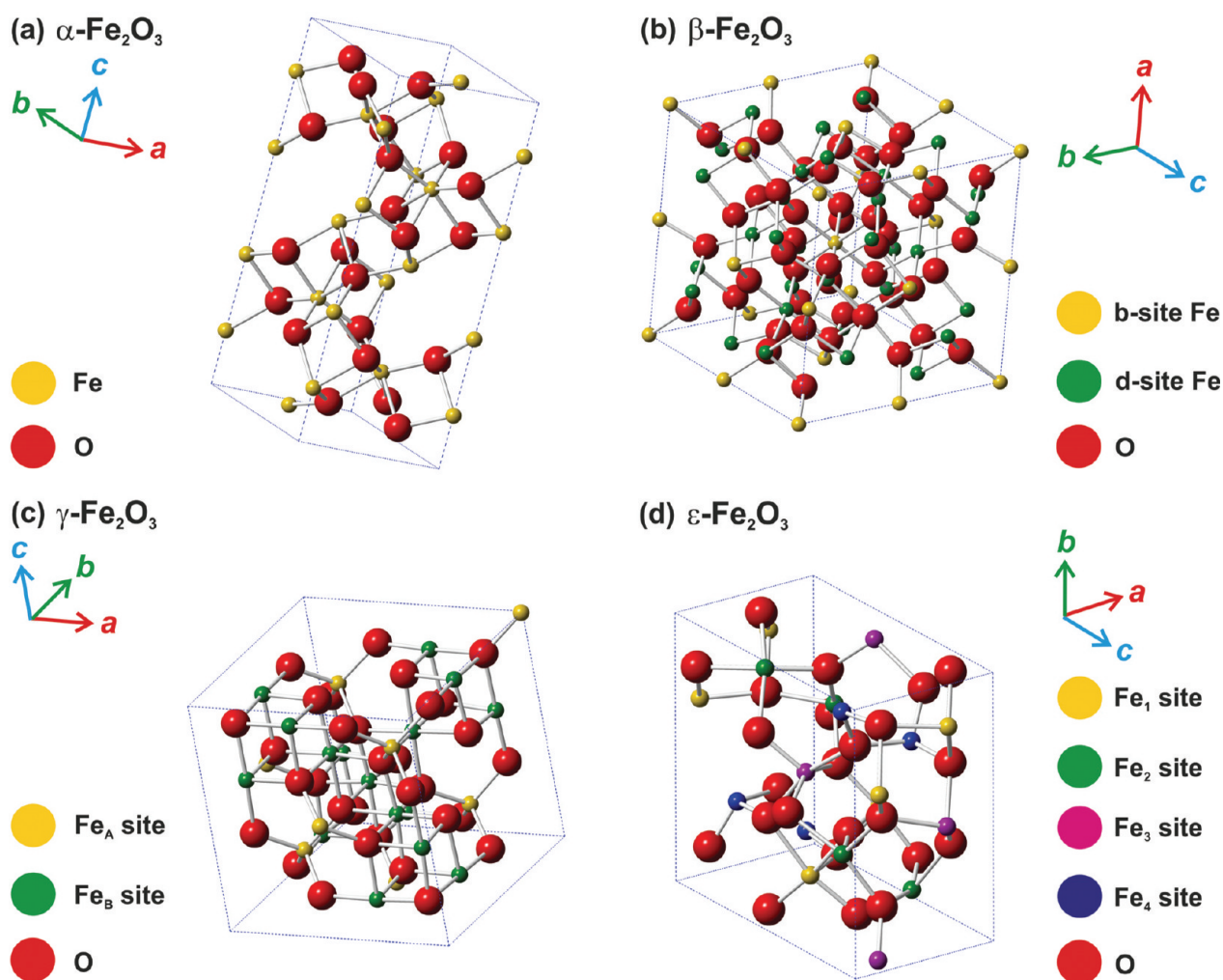


Figure 1. Graphical representations of the fundamental crystal structures of Fe_2O_3 : (a) $\alpha\text{-Fe}_2\text{O}_3$, (b) $\beta\text{-Fe}_2\text{O}_3$, (c) $\gamma\text{-Fe}_2\text{O}_3$, (d) $\varepsilon\text{-Fe}_2\text{O}_3$.

octahedral sites are occupied by $\text{Fe}(\text{III})$ ions (see Figure 1). It crystallizes in the $R\bar{3}c$ space group, with lattice parameters $a = 5.036 \text{ \AA}$ and $c = 13.749 \text{ \AA}$, and six formula units per unit cell. It has unusual magnetic properties, with two magnetic transition temperatures. The basal plane of the $\alpha\text{-Fe}_2\text{O}_3$ crystal structure contains two interpenetrating magnetic sublattices. Below $\sim 260 \text{ K}$ (in the case of bulk and pure $\alpha\text{-Fe}_2\text{O}_3$ without cation substitution), it behaves as an ideal antiferromagnet with the spins lying along the electric field gradient (oriented nearly along the $\alpha\text{-Fe}_2\text{O}_3$ c -crystallographic axis). At $\sim 260 \text{ K}$ (known as the Morin transition temperature), the spins are reoriented by $\sim 90^\circ$ so as to lie approximately in the $\alpha\text{-Fe}_2\text{O}_3$ basal plane.^{15,16} Adjacent spins belonging to different magnetic sublattices are aligned in an almost antiparallel manner; they are canted by about 5° , leaving a weak ferromagnetic moment pointing in a direction perpendicular to the basal plane. Thus, above $\sim 260 \text{ K}$, $\alpha\text{-Fe}_2\text{O}_3$ is said to behave as a weak ferromagnet or a canted antiferromagnet. It should be noted that the Morin transition temperature is sensitive to a number of factors including particle size, lattice defects, the presence of impurities and/or ion substitution.^{1,2,17–19} In the case of extremely small nanoparticles of $\alpha\text{-Fe}_2\text{O}_3$ (typically, those with diameters below 20 nm), the Morin transition is suppressed below 4.2 K. Above 950 K (the Néel temperature of $\alpha\text{-Fe}_2\text{O}_3$), $\alpha\text{-Fe}_2\text{O}_3$ loses its magnetic ordering and becomes a paramagnet. $\alpha\text{-Fe}_2\text{O}_3$ is one of the final products of the

thermal conversion or decomposition of a variety of iron(II)- and iron(III)-containing compounds as well as the final product of thermally induced transformations of other iron oxides and/or structural transformations of other Fe_2O_3 polymorphs.²⁰ Therefore, $\alpha\text{-Fe}_2\text{O}_3$ is more easy to synthesize than other forms of Fe_2O_3 . Historically, one of the first uses of $\alpha\text{-Fe}_2\text{O}_3$ was in the production of red pigments.^{1,21,22} More recently, thin films of $\alpha\text{-Fe}_2\text{O}_3$ have been demonstrated to be viable semiconducting photoanodes for solar hydrogen production through water splitting^{23–33} and for solar oxygen evolution from SO_4^{2-} ions.³⁴ $\alpha\text{-Fe}_2\text{O}_3$ has some significant advantages as a photoelectrode in solar cells, including its suitable bandgap, high resistance to corrosion, and low cost. In addition, $\alpha\text{-Fe}_2\text{O}_3$ has proved to be an effective and selective gas sensor for the detection of oxygen, ethanol, formaldehyde, and other gases based on changes in its surface resistivity in the presence of gas.^{35–40} Nanostructures of $\alpha\text{-Fe}_2\text{O}_3$ have been successfully used as heterogeneous catalysts in the degradation^{41,42} and alkylation of phenols,⁴³ as highly efficient and selective catalysts in the oxidation of cyclohexane,⁴⁴ and to promote the decomposition of hydrogen peroxide.⁴⁵ Nanoparticles of $\alpha\text{-Fe}_2\text{O}_3$ coated with gold nanoparticles are potent catalysts of CO oxidation.^{46–49} Recently, solid solutions of $\alpha\text{-Fe}_2\text{O}_3$ and FeTiO_3 have been used as model systems to explain the remanent magnetism (which is driven by so-called lamellar magnetism) exhibited by rocks and soils found on

extraterrestrial objects (planets, asteroids, etc.). It turns out that $(\text{FeTiO}_3)_x(\alpha\text{-Fe}_2\text{O}_3)_{1-x}$ ($0.50 \leq x \leq 0.75$) solid solutions possess a remanent magnetization that is extremely strong and time-stable.^{22,50} When formed in nature, the magnetic state of such solid solutions, usually consisting of $\alpha\text{-Fe}_2\text{O}_3$ and FeTiO_3 lamellae with one or more dimensions in a nanometer scale, is affected by a magnetic field (of a planetary body) to which they are exposed. Commonly, they obstruct to adopt the present planet magnetic field and thus reflect the magnetic history of the planetary body. In addition, these solid solutions exhibit an exchange bias (manifested by an exchange bias field of more than 1 T), which supports the theory of lamellar magnetism in natural systems made up of lamellae that have grown into a host mineral.⁵¹ However, from the viewpoint of magnetism-based applications, $\alpha\text{-Fe}_2\text{O}_3$ nanoparticles are not considered as suitable magnetic candidates due to the small magnetic moment they exhibit.

1.2. $\beta\text{-Fe}_2\text{O}_3$. $\beta\text{-Fe}_2\text{O}_3$ is a rare polymorph of iron(III) oxide that exists only in nanosized form; its natural abundance has yet to be reported. $\beta\text{-Fe}_2\text{O}_3$ exhibits a body-centered cubic “bixbyite” structure and crystallizes in the $Ia\bar{3}$ space group with $a = 9.393 \text{ \AA}$. In $\beta\text{-Fe}_2\text{O}_3$, the Fe(III) ions occupy two nonequivalent octahedral crystallographic sites (see Figure 1). $\beta\text{-Fe}_2\text{O}_3$ is the only iron(III) oxide polymorph that exhibits paramagnetic behavior at room temperature; its Néel magnetic transition temperature is between 100 and 119 K. Below this temperature, $\beta\text{-Fe}_2\text{O}_3$ is antiferromagnetically ordered. Because it is thermodynamically unstable, it is transformed into either $\alpha\text{-Fe}_2\text{O}_3$ (refs 52–55) or $\gamma\text{-Fe}_2\text{O}_3$ (ref 56) on heating, depending on the precise nature of the nanoparticles. To date, $\beta\text{-Fe}_2\text{O}_3$ has found few applications. Recently, $\beta\text{-Fe}_2\text{O}_3$ nanoparticles prepared by solid-state synthesis⁵² have been incorporated into a carbon paste and tested as an electro-catalyst for the reduction of hydrogen peroxide.⁵⁷ Lee et al. studied the optoelectronic properties of hollow $\beta\text{-Fe}_2\text{O}_3$ nanoparticles;⁵⁸ the particles’ optical transmittance was found to be less than 40% in the visible-light region. In addition, Zboril et al.⁵⁹ have reported that the admixture of $\beta\text{-Fe}_2\text{O}_3$ has a noticeable effect on the quality of red ferric pigments.

1.3. $\gamma\text{-Fe}_2\text{O}_3$. $\gamma\text{-Fe}_2\text{O}_3$ (mineralogically known as maghemite) is the second most common Fe_2O_3 polymorph in nature and can be formed by a wide range of reactions. Like $\alpha\text{-Fe}_2\text{O}_3$, it exists in both bulk and nanosized forms. $\gamma\text{-Fe}_2\text{O}_3$ possesses a cubic crystal structure of an inverse spinel type and crystallizes in the $P4_132$ space group with $a = 8.351 \text{ \AA}$. Like Fe_3O_4 , it contains cations in two nonequivalent crystallographic sites, i.e., the tetrahedral (A) and octahedral (B) positions. Unlike Fe_3O_4 , the crystal structure of $\gamma\text{-Fe}_2\text{O}_3$ features vacant cation sites (\square), which usually occur in octahedral positions, to compensate for its increased positive charge (see Figure 1). Thus, the stoichiometry of $\gamma\text{-Fe}_2\text{O}_3$ can be formally described as $\text{Fe}^{\text{A}}(\text{Fe}_{5/3}\square_{1/3})^{\text{B}}\text{O}_4$. However, at least three different crystal $\gamma\text{-Fe}_2\text{O}_3$ symmetries have been reported, depending on the extent and nature of the ordering of the vacancies in the octahedral sites of the $\gamma\text{-Fe}_2\text{O}_3$ crystal structure: (i) a cubic vacancy-disordered structure ($Fd\bar{3}m$ crystal space group) in which the vacancies are randomly distributed, (ii) a cubic vacancy-ordered structure ($P4_332$ and/or $P4_132$ crystal space group) exhibiting a partially ordered vacancy pattern, and (iii) a tetragonal structure with a threefold doubling along the c -axis and perfectly ordered vacancies ($P4_3212$ crystal space group, $a = 8.349 \text{ \AA}$, $c = 24.996 \text{ \AA}$).^{60–65} Because it has a spinel structure with two magnetic sublattices, $\gamma\text{-Fe}_2\text{O}_3$ is a typical ferrimagnetic material like Fe_3O_4 ; it is readily magnetized

and thus has a high magnetic response when placed in an external magnetic field. Ultrafine particles of $\gamma\text{-Fe}_2\text{O}_3$ (i.e., those with sizes of $\sim 10 \text{ nm}$ or less) exhibit superparamagnetic relaxation. In fact, $\gamma\text{-Fe}_2\text{O}_3$ was one of the materials that prompted the development of the theory of superparamagnetism, and it has been studied extensively in this context.^{66–74} Superparamagnetism is a thermally activated relaxation phenomenon that is typically observed in nanoscale structures, in which the particle’s overall magnetic moment (i.e., superspin) spontaneously fluctuates between various orientations that are energetically favored by its magnetic (magnetocrystalline in most cases) anisotropy. Nanosized $\gamma\text{-Fe}_2\text{O}_3$ is a very useful material in nanotechnological applications because its nanoparticles have interesting magnetic and surface properties and it is nontoxic, biodegradable, biocompatible, and chemically stable. Therefore, in addition to their widespread use in the magnetic recording industry and chemistry, ultrafine $\gamma\text{-Fe}_2\text{O}_3$ particles have also found applications in biomedicine and biotechnology. These include the immobilization and modification of biologically active compounds, the magnetic isolation and separation of labeled cells, magnetic targeting of drugs and radionuclides (i.e., controlled drug delivery), magnet-induced tumor treatment via hyperthermia, and the determination of biologically active compounds and xenobiotics; they have also been used as contrast agents for nuclear magnetic resonance imaging.^{14,75–82} Like $\beta\text{-Fe}_2\text{O}_3$, $\gamma\text{-Fe}_2\text{O}_3$ is thermodynamically unstable and is converted either directly or indirectly (with $\varepsilon\text{-Fe}_2\text{O}_3$ as an intermediate product) to $\alpha\text{-Fe}_2\text{O}_3$ when the temperature exceeds a threshold value; the precise value of this threshold is dependent on several physicochemical parameters.

1.4. $\varepsilon\text{-Fe}_2\text{O}_3$. Like $\beta\text{-Fe}_2\text{O}_3$, $\varepsilon\text{-Fe}_2\text{O}_3$ is a rare Fe_2O_3 polymorph that exists only in the form of nanostructures and whose natural abundance is low.³ $\varepsilon\text{-Fe}_2\text{O}_3$ has an orthorhombic crystal structure with the $Pna2_1$ space group and lattice parameters $a = 5.095 \text{ \AA}$, $b = 8.789 \text{ \AA}$, and $c = 9.437 \text{ \AA}$.³ The $\varepsilon\text{-Fe}_2\text{O}_3$ crystal structure derives from a close packing of four oxygen layers. The structure itself (see Figure 1) consists of triple chains of octahedra sharing edges and simple chains of tetrahedra sharing corners which run parallel to the crystallographic a -axis. It has six crystallographically nonequivalent anion and four cation (Fe_1 , Fe_2 , Fe_3 , and Fe_4) positions;^{83,84} in contrast to $\gamma\text{-Fe}_2\text{O}_3$, all of the cation positions are filled with Fe^{3+} ions, leaving no vacancies in the crystal structure. The Fe_4 cation position is tetrahedrally coordinated; the other three cation positions (i.e., Fe_1 , Fe_2 , and Fe_3) are octahedrally coordinated. All of the cation polyhedra exhibit a certain degree of distortion;⁸⁴ this is believed to be crucial for the magnetic properties of $\varepsilon\text{-Fe}_2\text{O}_3$ and their evolution as the temperature is reduced.^{3,85} On the basis of the distortion of the polyhedra, the Fe_1 and Fe_2 sites are said to possess a distorted octahedral coordination while the Fe_3 sites have regular octahedral coordination.^{3,84} Interestingly, as in $\alpha\text{-Fe}_2\text{O}_3$, all of the oxygen layers contain the same percentage of iron, i.e., 0.67 Fe per atom of oxygen. As in $\gamma\text{-Fe}_2\text{O}_3$, oxygen “sandwiches” containing six-coordinated iron alternate with oxygen “sandwiches” containing six- and four-coordinated iron. Thus, $\varepsilon\text{-Fe}_2\text{O}_3$ can be regarded as an intermediate polymorph, having similarities to both $\gamma\text{-Fe}_2\text{O}_3$ and $\alpha\text{-Fe}_2\text{O}_3$. However, its magnetic behavior is not fully understood.³ So far, it has been reported to undergo two magnetic transitions, one taking place at $\sim 495 \text{ K}$ (which is its Curie temperature) and the other at $\sim 110 \text{ K}$ as the temperature decreases.³ At the $\sim 495 \text{ K}$ transition, $\varepsilon\text{-Fe}_2\text{O}_3$ goes from a paramagnetic to a magnetically ordered state. At $\sim 110 \text{ K}$, it undergoes a transition from this

magnetically ordered state to another magnetic regime, distinct from that observed at room temperature. At room temperature, $\varepsilon\text{-Fe}_2\text{O}_3$ behaves either as a collinear ferrimagnet^{3,83,84,86–88} or as a canted antiferromagnet.^{3,89,90} A dispute exists concerning the low temperature magnetic state of $\varepsilon\text{-Fe}_2\text{O}_3$. At ~ 110 K, $\varepsilon\text{-Fe}_2\text{O}_3$ undergoes a magnetic transition either from the ferrimagnetic state to some incommensurate magnetic structure (probably of a square-wave-modulated origin)^{3,84} or from one canted antiferromagnetic state to another (with a different canting angle); it may exhibit metamagnetic behavior at low temperatures.^{3,89,90} Nevertheless, irrespective of the proposed nature of the room-temperature and low-temperature magnetic ground states of $\varepsilon\text{-Fe}_2\text{O}_3$, all of those who work with this remarkable iron oxide polymorph agree that the transition at ~ 110 K is accompanied by a series of structural transformations and spin reorientation phenomena.³ $\varepsilon\text{-Fe}_2\text{O}_3$ is one of the more remarkable iron oxide polymorphs because it exhibits a giant coercive field of ~ 2 T at room temperature.⁸⁶ In the light of the recent studies, this large room-temperature coercivity of $\varepsilon\text{-Fe}_2\text{O}_3$ is believed to be a consequence in particular of $\varepsilon\text{-Fe}_2\text{O}_3$ disordered structure.⁸⁵ Besides this, $\varepsilon\text{-Fe}_2\text{O}_3$ possesses a large magnetocrystalline anisotropy driven by an establishment of a single-domain character due to conveniently sized $\varepsilon\text{-Fe}_2\text{O}_3$ nanoobjects and a nonzero orbital component of the Fe^{3+} magnetic moment, explaining the existence of significant spin–orbit coupling.^{85,86} The nonzero orbital moment is related to the observed distortions in the coordination polyhedra of Fe_1 and Fe_2 sites which probably result in $\text{Fe}(3\text{d})-\text{O}(2\text{p})$ mixing and $\text{O}(2\text{p})$ -to- $\text{Fe}(3\text{d})$ charge transfer that, along with the crystal-field effects, lift the electronic degeneracy in the d orbitals, leading to an electronic state where the angular momentum is no longer zero as expected in Fe^{3+} (refs 3 and 85). However, at ~ 110 K, the coercivity of $\varepsilon\text{-Fe}_2\text{O}_3$ is dramatically reduced; this is probably a consequence of the reduced spin–orbit coupling associated with the structural and magnetic (spin arrangement) transformations that accompany this magnetic transition.⁸⁵ Its giant room-temperature coercive field makes $\varepsilon\text{-Fe}_2\text{O}_3$ a potentially attractive material for use in high-coercivity recording media; its magnetoelectric coupling⁹¹ and millimeter-wave ferromagnetic resonance^{92,93} could also make it useful in a wide range of other applications including electric/magnetic field tunable devices and fields where an effective suppression of the electromagnetic interference and a stabilization of the electromagnetic transmittance are required. However, it is very difficult to synthesize samples of this nanomaterial that are not contaminated with other iron oxide phases.³ So far, only one synthetic route for the production of $\varepsilon\text{-Fe}_2\text{O}_3$ with no traces of other iron oxide impurities has been reported (for details, see Tucek et al.³). Other problems associated with the synthesis of $\varepsilon\text{-Fe}_2\text{O}_3$ include low yields and the material's significant thermal instability (upon heating, it is readily converted to $\alpha\text{-Fe}_2\text{O}_3$). Because $\varepsilon\text{-Fe}_2\text{O}_3$ is a metastable intermediate phase, a deep understanding of Fe_2O_3 polymorphism will be required if a controlled and reliable method for its synthesis is to be developed.

1.5. Methods of Inducing Polymorphous Transitions in Fe_2O_3 . There are two main methods by which polymorphous transformations of Fe_2O_3 can be induced: mechanical and thermal treatment. Mechanical activation can be achieved either by high pressure treatment or by milling, while thermal treatment involves isothermal or dynamic heating. The mechanism of the polymorphous transformation of Fe_2O_3 depends not only on the applied physicochemical conditions but also on the form of the ferric oxide sample (crystals, nanopowder, nanocomposite, thin film, coated particles, etc.), as summarized in Table 1. Other

Table 1. Summary of the Important Properties and Forms of Fe_2O_3 Samples and Parameters That Affect Their Polymorphous Transformations

| particle properties | material form | transition inducing parameters |
|------------------------------|--------------------|--------------------------------|
| crystal structure | free bulk crystals | temperature |
| particle size (distribution) | (nano)powder | pressure |
| particle morphology | thin film | milling |
| crystallinity (amorphicity) | nanocomposite | laser irradiation |
| degree of agglomeration | coated particles | |

factors that have a significant effect on the outcome of the polymorphous transformation include the internal properties of the particles (structure, crystallinity) as well as external parameters (particle morphology, the degree of particle aggregation, and the particles' size distribution). A full understanding of the mechanisms of the polymorphous transitions of Fe_2O_3 would thus be useful in basic research and in the development of methods for the controlled synthesis of single-phased Fe_2O_3 polymorphs.

2. POLYMORPHOUS TRANSITIONS OF $\gamma\text{-Fe}_2\text{O}_3$

As already mentioned, $\gamma\text{-Fe}_2\text{O}_3$ exists in both bulk and nanosized forms. $\gamma\text{-Fe}_2\text{O}_3$ frequently occurs in nature, and numerous synthetic methods for its preparation have been reported, all of which give rise to particles with different average sizes, size distributions, morphologies, degrees of agglomeration, and magnetic properties. Of the known Fe_2O_3 polymorphs, $\gamma\text{-Fe}_2\text{O}_3$ is regarded as the most practically important and useful due to its simple synthesis and the interesting magnetic characteristics of its nanosized objects. Consequently, considerable effort has been expended on developing new methods for the preparation of nanosized $\gamma\text{-Fe}_2\text{O}_3$, mostly in the form of nanopowders, nanocomposites, nanowires,⁹⁴ nanotubes,^{95,96} coated (functionalized) nanoparticles, and/or thin films. Numerous synthetic techniques have been used in the preparation of $\gamma\text{-Fe}_2\text{O}_3$ nanoobjects, including laser pyrolysis, coprecipitation, electrochemistry, sol–gel methods, aerosol techniques, microemulsion methods with ionic surfactants, and physical methods such as ball-milling and film deposition, sonochemistry, spray pyrolysis techniques, and/or microwave plasma methods.¹⁴ Many $\gamma\text{-Fe}_2\text{O}_3$ syntheses involve the thermal decomposition of suitable iron-containing precursors such as iron(II) pentacarbonyl,^{97,98} iron(II) oxalate dihydrate, ferrocene,⁹⁹ gluconate dihydrate,¹⁰⁰ or iron(II) acetonacetate.¹⁰¹ An understanding of the thermal stability of $\gamma\text{-Fe}_2\text{O}_3$ toward polymorphous transformations during its synthesis and use is therefore highly important.

2.1. Effects of Particle Size. It is generally known that $\gamma\text{-Fe}_2\text{O}_3$ is thermally unstable at elevated temperatures and undergoes an irreversible transformation to $\alpha\text{-Fe}_2\text{O}_3$ (the first brief review of this topic can be found in the book by Cornell and Schwertmann¹). The temperature at which this occurs and the mechanism and kinetics of the process are primarily dependent on the size and morphology of the particles involved, the form of the material (powder, nanocomposite, thin film, coated particles, or core–shell particles, as well as the potential use of cation doping in the $\gamma\text{-Fe}_2\text{O}_3$ crystal structure), its “history”, and the atmosphere under which the phase transformation happens. The direct $\gamma\text{-Fe}_2\text{O}_3$ -to- $\alpha\text{-Fe}_2\text{O}_3$ polymorphous transformation pathway has been observed in powdered

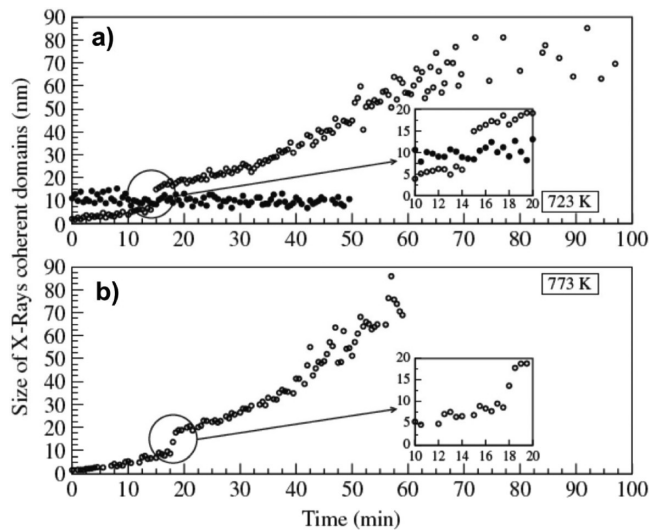


Figure 2. Sizes of the X-ray coherent domains of $\alpha\text{-Fe}_2\text{O}_3$ (empty circle) and $\gamma\text{-Fe}_2\text{O}_3$ (black circle) phases during the $\gamma\text{-Fe}_2\text{O}_3$ -to- $\alpha\text{-Fe}_2\text{O}_3$ transition. $\gamma\text{-Fe}_2\text{O}_3$ samples (particle size of about 9 ± 1 nm) were heated at (a) 723 and (b) 773 K. An enormous increase in the sizes of the X-ray coherent domains (from 9 to 18 nm) was detected (see enlargement). Reprinted with permission from Belin et al.¹¹¹ Copyright 2007 Elsevier.

materials in the absence of a matrix.^{102–109} Thus, the kinetics of the phase transformation from powdered nanocrystalline (9–16 nm) $\gamma\text{-Fe}_2\text{O}_3$ to $\alpha\text{-Fe}_2\text{O}_3$ was observed by *in situ* X-ray powder diffraction (XRD) measurements at temperatures around 300 °C.¹⁰² The sizes of the formed $\alpha\text{-Fe}_2\text{O}_3$ crystals were above 35 nm, but no growth of the $\gamma\text{-Fe}_2\text{O}_3$ nanoparticles was observed during the heat treatment. A mixture of $\alpha\text{-Fe}_2\text{O}_3$ and superparamagnetic $\gamma\text{-Fe}_2\text{O}_3$ nanoparticles was prepared by thermal decomposition of $\text{FeC}_2\text{O}_4 \cdot 2\text{H}_2\text{O}$.¹⁰³ When the reaction time was increased, a $\gamma\text{-Fe}_2\text{O}_3$ -to- $\alpha\text{-Fe}_2\text{O}_3$ phase transformation was observed. It is remarkable that $\gamma\text{-Fe}_2\text{O}_3$ particles were formed only in the superparamagnetic state (at room temperature and with respect to the characteristic measurement time of Mössbauer spectroscopy). $\gamma\text{-Fe}_2\text{O}_3$ nanoparticles with an average crystal size of ~5 nm have been synthesized by the successive hydrolysis, oxidation, and dehydration of tetrapyridino-ferrous chloride.¹¹⁰ A direct transformation of nanocrystalline $\gamma\text{-Fe}_2\text{O}_3$ to micro-crystalline $\alpha\text{-Fe}_2\text{O}_3$ was observed during isothermal heat treatment at 385 °C. The conversion of $\gamma\text{-Fe}_2\text{O}_3$ to $\alpha\text{-Fe}_2\text{O}_3$ was studied *in situ* and in real-time by Belin et al., using synchrotron radiation.¹¹¹ These workers observed an abrupt doubling in the size of the X-ray coherent domains of $\alpha\text{-Fe}_2\text{O}_3$ when heating the $\gamma\text{-Fe}_2\text{O}_3$ precursor at either 723 or 773 K (see Figure 2).

Changes in particle size during $\gamma\text{-Fe}_2\text{O}_3$ -to- $\alpha\text{-Fe}_2\text{O}_3$ phase transformations have been reported by a number of authors, including Yen et al.,¹⁰⁹ Schimanke and Martin,¹⁰² Zboril et al.,¹⁰³ Belin et al.,¹¹¹ and Ennas et al.,¹¹⁰ suggesting that the polymorphous transformations may be particle size-induced. This suggestion is based on the hypothesis that the formation of $\alpha\text{-Fe}_2\text{O}_3$ is driven by heat-induced increases in the size of the nanocrystalline $\gamma\text{-Fe}_2\text{O}_3$ particles; the $\gamma\text{-Fe}_2\text{O}_3$ -to- $\alpha\text{-Fe}_2\text{O}_3$ phase conversion takes place once the $\gamma\text{-Fe}_2\text{O}_3$ nanoparticles reach a certain critical size (usually between 10 and 25 nm).^{102,103,109,111} An illustrative example is shown in Figure 3, which depicts the results obtained by Zboril et al.¹⁰³ in their study

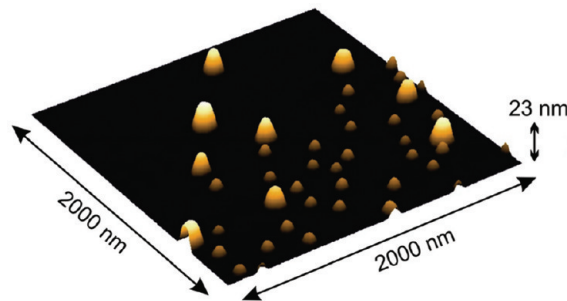


Figure 3. Atomic force microscopy image showing two types of nanoparticles: smaller particles with vertical dimensions between 4 and 7 nm consist of $\gamma\text{-Fe}_2\text{O}_3$, while larger particles with a vertical dimension between 16 and 22 nm consist of $\alpha\text{-Fe}_2\text{O}_3$ formed by thermally induced phase transformation of $\gamma\text{-Fe}_2\text{O}_3$. Reprinted with permission from Zboril et al.¹²⁷ Copyright 2002 Springer.

of two well-resolved types of nanoparticles using atomic force microscopy (AFM). The smaller particles, whose vertical dimensions are between 4 and 7 nm, consist of $\gamma\text{-Fe}_2\text{O}_3$; the larger ones (whose vertical dimensions are between 16 and 22 nm) consist of $\alpha\text{-Fe}_2\text{O}_3$ formed by a thermally induced phase transformation of $\gamma\text{-Fe}_2\text{O}_3$. In this study, $\gamma\text{-Fe}_2\text{O}_3$ and $\alpha\text{-Fe}_2\text{O}_3$ were identified and quantified using XRD and Mössbauer spectroscopy prior to the AFM measurements.¹⁰³ The diffraction lines originating from the $\gamma\text{-Fe}_2\text{O}_3$ particles were broader than those corresponding to $\alpha\text{-Fe}_2\text{O}_3$, confirming the smaller size of the $\gamma\text{-Fe}_2\text{O}_3$ particles. It is instructive to consider the thermodynamic aspects of this phenomenon: under any given set of conditions, there is a “competition” between the particle’s surface energy and the activation energy of the system. Both of these energies are very closely related to the particle size. Navrotsky et al.¹¹² have published a review paper that discusses the effects of particle size and hydration on the occurrence and stability of various iron oxides and report a limiting value of 16 nm for the thermodynamic stability of nanosized anhydrous $\gamma\text{-Fe}_2\text{O}_3$ particles; this is consistent with the observations of Zboril et al.¹⁰³ However, there are some apparent inconsistencies in the data reported in the literature. Thus, Gnanaprakash et al.¹¹³ claim that the $\gamma\text{-Fe}_2\text{O}_3$ -to- $\alpha\text{-Fe}_2\text{O}_3$ phase transition temperature decreases as the particle size falls, due to a reduction in the activation energy of the system, while Ye et al.¹¹⁴ reported that the transition temperature of nanocrystalline $\gamma\text{-Fe}_2\text{O}_3$ is higher than that of its coarse-grained counterpart. In our experience, it is generally the case that smaller nanoparticles of nanopowdered $\gamma\text{-Fe}_2\text{O}_3$ have lower transition temperatures.

2.2. Effects of Coating and Doping. In addition to the effects of particle size discussed above, the $\gamma\text{-Fe}_2\text{O}_3$ -to- $\alpha\text{-Fe}_2\text{O}_3$ phase transition temperature can also be influenced by the particles’ morphology,⁵⁶ the presence of a coating layer on the particle surface,^{104,115} and the presence of dopants in the $\gamma\text{-Fe}_2\text{O}_3$ crystal structure.^{116,117} $\gamma\text{-Fe}_2\text{O}_3$ nanoparticles prepared by the structural transformation of hollow $\beta\text{-Fe}_2\text{O}_3$ nanoparticles exhibited high thermal stability toward conversion to $\alpha\text{-Fe}_2\text{O}_3$ even at 800 °C.⁵⁶ It was suggested that this high stability was due to the very large quantity of thermal energy required to reduce the hollow nanoparticles’ high surface area. Xu et al.¹¹⁵ prepared mono-disperse superparamagnetic SnO_2 -coated Fe_2O_3 nanoparticles and found that they exhibited enhanced thermal stability toward the phase transformation to $\alpha\text{-Fe}_2\text{O}_3$. They suggested that the SnO_2 shell acts as a barrier that hindered the growth of the

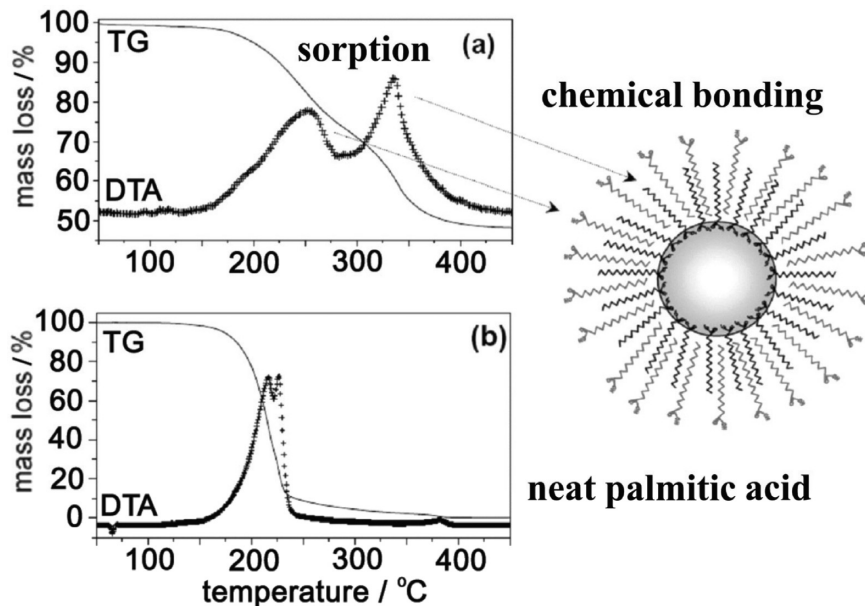


Figure 4. TG and DTA curves of (a) $\gamma\text{-Fe}_2\text{O}_3$ capped with palmitic acid and (b) neat palmitic acid in air. No effect corresponding to the $\gamma\text{-Fe}_2\text{O}_3$ -to- $\alpha\text{-Fe}_2\text{O}_3$ phase transformation is observed on DTA below 400 °C. Reprinted with permission from Zboril et al.¹¹⁸ Copyright 2008 Institute of Physics Publishing.

$\gamma\text{-Fe}_2\text{O}_3$ particles and thus prevented the $\gamma\text{-Fe}_2\text{O}_3$ -to- $\alpha\text{-Fe}_2\text{O}_3$ phase conversion from occurring at temperatures below 600 °C. The $\gamma\text{-Fe}_2\text{O}_3$ -to- $\alpha\text{-Fe}_2\text{O}_3$ phase transition temperature can be increased by ~100 °C by Zn^+ doping.¹¹⁶ Similarly, Y_2O_3 -doped $\gamma\text{-Fe}_2\text{O}_3$ is thermally stable at temperatures of up to 725 °C, which made it possible to use this material as a gas sensor with long-term stability.¹¹⁷ Ninjabdar et al.¹⁰⁴ compared the thermal properties of $\gamma\text{-Fe}_2\text{O}_3$ /poly(methyl methacrylate) (PMMA) core–shell nanoparticles to those of caprylate-capped $\gamma\text{-Fe}_2\text{O}_3$ nanoparticles, with both particle types having an average core size of 4 nm. It was found that while the caprylate-coated $\gamma\text{-Fe}_2\text{O}_3$ nanoparticles underwent a polymorphous transformation to $\alpha\text{-Fe}_2\text{O}_3$ at 400 °C, the PMMA-coated $\gamma\text{-Fe}_2\text{O}_3$ nanoparticles were stable up to 500 °C. This difference was attributed to the greater thermal stability of PMMA relative to the caprylate coating; the presence of an intact coating is proposed to prevent the aggregation and structural transformation of the $\gamma\text{-Fe}_2\text{O}_3$ nanoparticles.

$\gamma\text{-Fe}_2\text{O}_3$ nanocrystallites functionalized with palmitic acid on their surface have also been shown to exhibit enhanced stability toward polymorphous transitions;¹¹⁸ the successful coating of the $\gamma\text{-Fe}_2\text{O}_3$ nanoparticles with palmitic acid was confirmed by thermal analysis. The thermogravimetric (TGA) and differential thermal analysis (DTA) curves of the palmitic acid-coated nanoparticles indicated that the coating undergoes a two-step decomposition process at temperatures below 400 °C (see Figure 4a), which suggests that palmitic acid interacts with the $\gamma\text{-Fe}_2\text{O}_3$ nanoparticles in two different ways. The first involves chemical bonding of the carboxylate group to Fe(III) ions on the particles' surface, while the second involves the physisorption of palmitic acid molecules, probably between adjacent coordinated palmitate units as shown schematically in Figure 4. For comparison, neat palmitic acid decomposes in what appears to be a single-step process at around 220 °C (see Figure 4b). Importantly, DTA provided no evidence of any exothermic effect consistent with a $\gamma\text{-Fe}_2\text{O}_3$ -to- $\alpha\text{-Fe}_2\text{O}_3$ polymorphous transformation at temperatures below 400 °C. The

coating thus increases the particles' transition temperature to some value above 400 °C.

2.3. Nano composites. The incorporation of $\gamma\text{-Fe}_2\text{O}_3$ nanoparticles into an amorphous and porous SiO_2 matrix was found to significantly alter the mechanism and kinetics of their thermal transformations. Several authors have independently observed $\gamma\text{-Fe}_2\text{O}_3$ to be much more thermally stable in a matrix;^{119–123} in air, it is only transformed to $\alpha\text{-Fe}_2\text{O}_3$ at temperatures above 900 °C, and the transformation occurs via an indirect mechanism that features $\varepsilon\text{-Fe}_2\text{O}_3$ as an intermediate. The porous SiO_2 matrix serves as an antisintering agent, which prolongs the life of the metastable $\varepsilon\text{-Fe}_2\text{O}_3$ and prevents its transformation to $\alpha\text{-Fe}_2\text{O}_3$ even at higher temperatures. This space restriction, together with the interactions between the silica and the particle surface, serves to limit the size of the $\varepsilon\text{-Fe}_2\text{O}_3$ nanoparticles, typically to less than 200 nm.¹²⁴ Consequently, $\varepsilon\text{-Fe}_2\text{O}_3$ is formed by the sintering of very limited numbers of $\gamma\text{-Fe}_2\text{O}_3$ nanoparticles. From a thermodynamic perspective, the decrease in the particles' surface area caused by sintering and agglomeration reduces the free energy of the system in the composites.¹²⁵ However, in contrast to the case with the powdered samples, the free energy cannot be fully minimized by further agglomeration because of the space limitations imposed by the matrix, and so metastable $\varepsilon\text{-Fe}_2\text{O}_3$ is formed instead of the otherwise more thermodynamically stable $\alpha\text{-Fe}_2\text{O}_3$. Above the so-called glass transition temperature (~1200 °C), amorphous silica softens; at 1470 °C, it crystallizes to cristobalite. This increases the space available to the incorporated $\varepsilon\text{-Fe}_2\text{O}_3$ nanoparticles, allowing further sintering, which is a prerequisite for their structural transformation to $\alpha\text{-Fe}_2\text{O}_3$. In addition to the thermal properties of the SiO_2 matrix, the relative proportion of iron(III) oxide in the nanocomposite (which is quantified in terms of the Fe/Si atomic ratio) also has a significant effect on the formation of $\varepsilon\text{-Fe}_2\text{O}_3$. Sartorato et al.¹²⁶ obtained almost pure $\varepsilon\text{-Fe}_2\text{O}_3$ in the case of the Fe/Si ratio being equal to 0.013, while in the case of higher Fe_2O_3 content (Fe/Si = 0.200), a mixture of $\varepsilon\text{-Fe}_2\text{O}_3$ and $\alpha\text{-Fe}_2\text{O}_3$ was observed even at

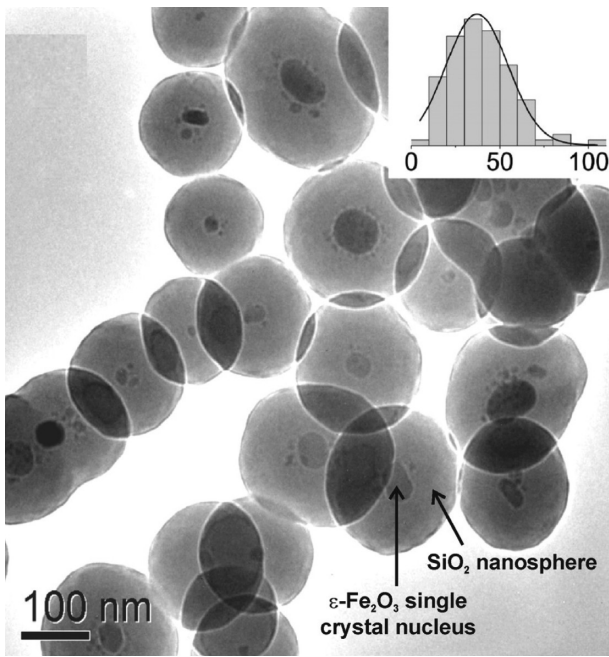


Figure 5. TEM image of ϵ - Fe_2O_3 particles wrapped in a silica shell. The inset shows the size distribution of the ϵ - Fe_2O_3 nanoparticles; their mean size was 37 nm, with 50% polydispersity. Reprinted with permission from Taboada et al.¹¹⁹ Copyright 2009 American Chemical Society.

300 °C. It was proposed that this happened because more sintered γ - Fe_2O_3 particles are needed to form α - Fe_2O_3 than is the case for ϵ - Fe_2O_3 .¹²⁶ This is entirely consistent with the results of Taboada et al.,¹¹⁹ who were able to prepare single crystals of ϵ - Fe_2O_3 individually wrapped in silica shells by the controlled recrystallization of γ - Fe_2O_3 nanoparticles (with a size of \sim 7 nm) that had been confined in silica shells by calcination in air at 1100 °C (see Figure 5).¹¹⁹ The thick and compact silica shells prevented the sintering of the γ - Fe_2O_3 nanoparticles and thereby inhibited their transformation to α - Fe_2O_3 .

In contrast to the situation with nanocomposites, the γ - $\text{Fe}_2\text{O}_3 \rightarrow \epsilon$ - $\text{Fe}_2\text{O}_3 \rightarrow \alpha$ - Fe_2O_3 phase transformation has not been observed in many studies on powdered materials. Zboril et al.¹²⁷ and Barcova et al.^{128,129} studied the thermally induced solid-state syntheses of γ - Fe_2O_3 nanoparticles using FeSO_4 , $\text{Fe}_2(\text{C}_2\text{O}_4)_3$, and almandine garnet precursors and their transformation to α - Fe_2O_3 via ϵ - Fe_2O_3 . All of the known crystalline polymorphs of Fe_2O_3 (α -, β -, γ -, and ϵ - Fe_2O_3) were observed during the thermal conversion of rhombohedral $\text{Fe}_2(\text{SO}_4)_3$.^{53,130} The conversion mechanism was found to be primarily dependent on the temperature, although Mössbauer spectroscopy revealed that the particle size also influenced the ratio of the different polymorphs formed. The kinetic data published by Zboril et al.¹³⁰ suggest that $\text{Fe}_2(\text{SO}_4)_3$ decomposes at 590 °C by two competing routes: (i) $\text{Fe}_2(\text{SO}_4)_3 \rightarrow \beta$ - $\text{Fe}_2\text{O}_3 \rightarrow \alpha$ - Fe_2O_3 and (ii) $\text{Fe}_2(\text{SO}_4)_3 \rightarrow \gamma$ - $\text{Fe}_2\text{O}_3 \rightarrow \epsilon$ - $\text{Fe}_2\text{O}_3 \rightarrow \alpha$ - Fe_2O_3 . There are striking similarities between the decomposition mechanisms described by Sakurai et al.⁵⁴ for nanocomposites (FeSO_4 used by those authors may undergo oxidation to $\text{Fe}_2(\text{SO}_4)_3$) and those suggested by Zboril et al.¹³⁰ for the powdered material. The difference lies mainly in the rate of polymorphous transformations. While the transformations proceed relatively rapidly in the case of the powdered material, the rare β - Fe_2O_3 and ϵ - Fe_2O_3 polymorphs

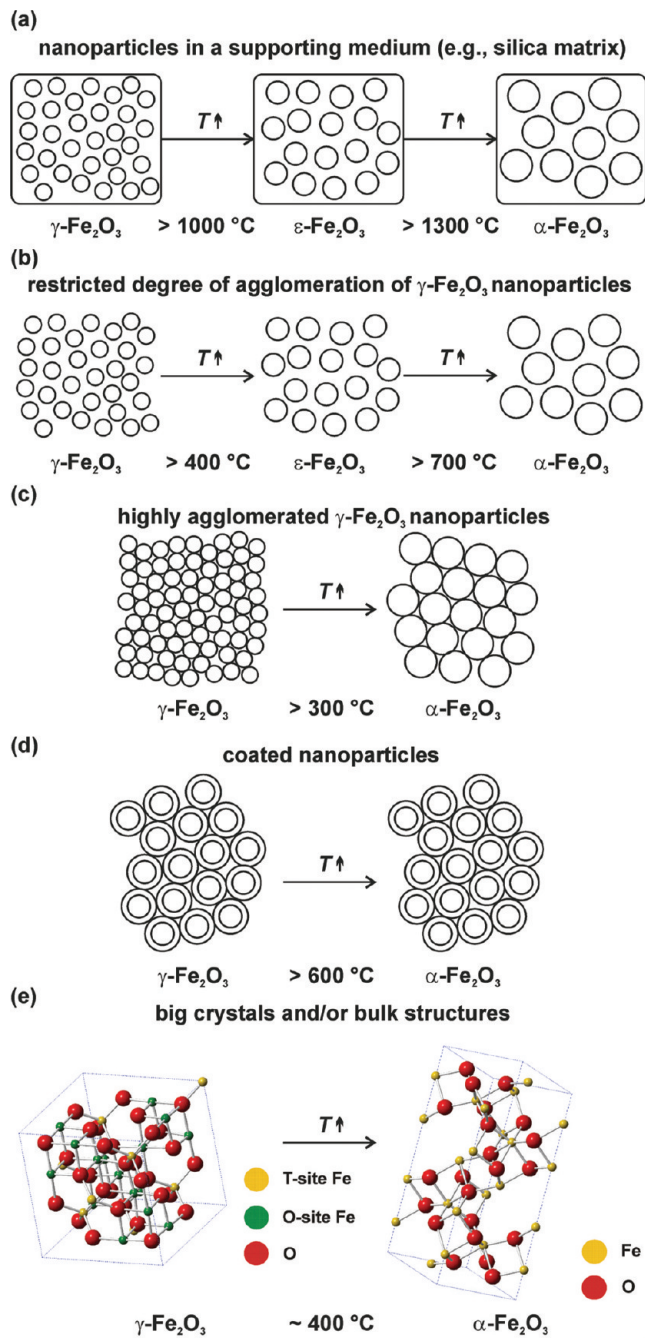


Figure 6. Schematic illustrations showing the mechanisms and temperature ranges of the thermally induced polymorphous transformation of γ - Fe_2O_3 .

are more thermally stable when incorporated into a matrix. This implies that pure ϵ - Fe_2O_3 can only be stabilized under certain conditions in a matrix and will be much more difficult to prepare as a powder. Generally, to obtain a pure ϵ - Fe_2O_3 phase by thermal decomposition, two things will be necessary: (i) a precursor with a sufficiently high decomposition temperature and (ii) adequate restrictions on the diffusion of the conversion gas and the agglomeration of ferric oxide nanoparticles formed within the nondecomposed microsized particles of the precursor (see Figure 6b). As a “negative” example, it is instructive to consider the oxidative decomposition of Prussian Blue, $\text{Fe}_4[\text{Fe}(\text{CN})_6]_3$,

which was shown to form the α -, β -, and γ - Fe_2O_3 polymorphs but not ε - Fe_2O_3 under any conditions. The relatively low decomposition temperature of Prussian Blue (about 250 °C) alone may be enough to cause the initially formed γ - Fe_2O_3 to be directly converted to α - Fe_2O_3 at temperatures above 400 °C.¹³¹

Because of its low cost and useful magnetic, semiconductive, and mechanical properties, considerable effort has been invested into the manufacture and application of thin films of iron(III) oxide. Recent research in this field has focused on the photocatalytic properties of thin films of α - Fe_2O_3 .^{24–29,132,133} Iron(III) oxide thin films have been deposited on fused quartz substrates by metal–organic deposition using Fe(III) acetylacetone as the organic precursor.¹³³ At a deposition temperature of 365 °C, γ - Fe_2O_3 with poor crystallinity was obtained. However, heat treatment at 800 °C resulted in the formation of polycrystalline α - Fe_2O_3 . The α - Fe_2O_3 film formed in this way promoted the photocatalytic degradation of an oxygenated aqueous solution of phenol upon illumination with visible light.¹³³ Very similar results were obtained by Aronniemi et al.¹³⁴ who prepared a thin film of γ - Fe_2O_3 on a glass substrate by gas phase deposition at 350 °C and then transformed it to α - Fe_2O_3 by heating at temperatures between 400 and 500 °C. Unfortunately, the authors did not mention which gas was used for the deposition. In general, one would expect thin films to have higher γ - Fe_2O_3 -to- α - Fe_2O_3 phase transformation temperatures than powders because of their comparatively limited scope for aggregation and particle growth.

In summary, the mechanism of the thermally induced polymorphous transformation of γ - Fe_2O_3 is primarily determined by the degree of agglomeration of the ferric oxide particles and the scope for particle growth. Thus, particle size-induced transformations result in the formation of ε - Fe_2O_3 in the presence of physical barriers that impede the particles' growth (such as are found in nanocomposites), but a direct γ - Fe_2O_3 -to- α - Fe_2O_3 phase transformation occurs when the particles are in close contact and agglomeration is not impeded. Figure 6 depicts some of the different forms of the γ - Fe_2O_3 precursor that can be used to control the phase transformation, including (a) a nanocomposite, (b) particles with a restricted degree of agglomeration, (c) aggregated particles, (d) coated nanoparticles, and (e) big crystals.

3. POLYMORPHOUS TRANSITIONS OF β - Fe_2O_3

β - Fe_2O_3 is an iron(III) oxide polymorph that has not been found in nature but has been synthesized as a powder,^{2,52} colloidal nanostructure,¹³⁵ hollow nanoparticles,^{136,137} and/or thin films.^{138,139} Interestingly, β - Fe_2O_3 is the only iron(III) oxide polymorph that exhibits paramagnetism at room temperature. The preparation of pure β - Fe_2O_3 is quite difficult; only a few synthetic methods for the preparation of pure, mostly nanosized β - Fe_2O_3 have been reported to date. Hollow β - Fe_2O_3 nanoparticles (20–40 nm) (see Figure 7) have been prepared by chemical vapor condensation using iron(III) acetylacetone as the precursor.¹³⁶ Colloidal β - Fe_2O_3 nanostructures with different shapes were synthesized by hydrolysis of FeCl_3 .¹³⁵ Pure β - Fe_2O_3 nanopowder can be prepared by a thermal solid-state reaction between NaCl and $\text{Fe}_2(\text{SO}_4)_3$ followed by separation of the byproduct.^{2,52} β - Fe_2O_3 films have been deposited on an Si wafer and fused with silica substrates by spray pyrolysis.¹³⁹ It was found that the thermal stability of the β - Fe_2O_3 film was significantly dependent on the presence of Si dopants. Iron(III) acetylacetone has also been used as a precursor for the chemical vapor

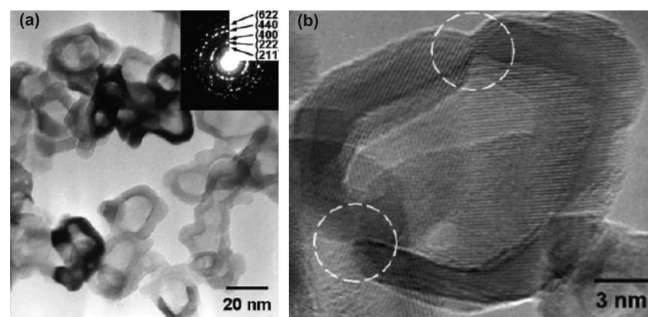


Figure 7. (a) TEM image of β - Fe_2O_3 hollow nanoparticles prepared by chemical vapor condensation; the selective area diffraction pattern in the inset confirms that the hollow nanoparticles consist of β - Fe_2O_3 . (b) HRTEM image displaying two nodes of the hollow nanoparticle, implying that the grain boundaries were formed at the junctions between two shells after nucleation and growth of the β - Fe_2O_3 phase. Reprinted with permission from Lee et al.¹³⁷ Copyright 2004 Springer.

deposition of a single phase β - Fe_2O_3 thin film at 600 °C under a flow of oxygen.¹³⁸ More commonly, β - Fe_2O_3 has been identified as a component of a mixture of Fe_2O_3 polymorphs;^{53,130,131} such mixtures may arise from the simultaneous formation of two Fe_2O_3 polymorphs (e.g., β - Fe_2O_3 and γ - Fe_2O_3) and/or polymorphous transformations of β - Fe_2O_3 and γ - Fe_2O_3 to α - Fe_2O_3 .

Several researchers have independently confirmed that the β - Fe_2O_3 polymorph is unstable at temperatures between 400 and 600 °C,^{52–55,58,139} with the precise decomposition temperature depending on the nature of the sample (powder, hollow nanostructure, or thin film). However, β - Fe_2O_3 is much more thermally stable than ε - Fe_2O_3 . In most of these studies, a direct thermally induced structural transformation of β - Fe_2O_3 to α - Fe_2O_3 was observed.^{52–55} Only in the case of β - Fe_2O_3 hollow nanoparticles, phase transformation to γ - Fe_2O_3 has been proved to occur at 400 °C.⁵⁶ This anomalous behavior was suggested to be a consequence of the hollow nanoparticles' high specific surface area. It would be very interesting to investigate the magnetic behavior and morphology of γ - Fe_2O_3 prepared from hollow β - Fe_2O_3 nanoparticles. If the particles' hollow morphology were preserved during the polymorphous transformation, the so-formed γ - Fe_2O_3 would be a rather unique nanomaterial that could be expected to have unusual magnetic properties.

Powdered β - Fe_2O_3 was observed to undergo a phase transformation to α - Fe_2O_3 at 590 °C in a study of the mechanism of the thermal decomposition of $\text{Fe}_2(\text{SO}_4)_3$ in air.^{53,130} Interestingly, ferric sulfate is the only known precursor from which all four polymorphs of Fe_2O_3 can be prepared by thermal decomposition, albeit as a mixture. As might be expected, β - Fe_2O_3 dispersed in an SiO_2 matrix exhibits significantly increased thermal stability, undergoing the transformation to α - Fe_2O_3 at 1200 °C according to Sakurai et al.⁵⁴ Thus, nanopowders and thin films of β - Fe_2O_3 are transformed to α - Fe_2O_3 , while hollow nanoparticles of β - Fe_2O_3 are transformed to γ - Fe_2O_3 (see the scheme in Figure 8).

4. ε - Fe_2O_3 AS AN INTERMEDIATE ON THE POLYMORPHOUS ROUTE FROM γ - Fe_2O_3 TO α - Fe_2O_3

Like β - Fe_2O_3 , ε - Fe_2O_3 exists only as nanoscaled objects. The reason for this is related to its low surface energy,¹²¹ which means that surface effects have a profound influence on the formation and existence of ε - Fe_2O_3 . To date, ε - Fe_2O_3 has been synthesized

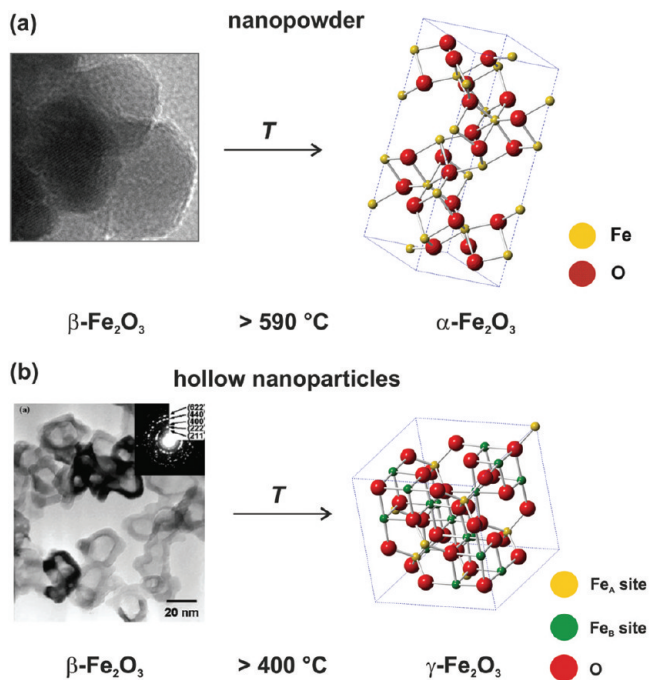


Figure 8. Schematic illustrations showing how the mechanisms of the thermally induced polymorphous transformation of $\beta\text{-Fe}_2\text{O}_3$ vary depending on particle morphology.

in the form of thin films and nanoparticles having a spherical (sphere-like) and/or nanorod (nanowire) morphology.³ Frequently, the size distribution of nanosphere-, nanorod-, and nanowire-shaped $\varepsilon\text{-Fe}_2\text{O}_3$ is found to be dependent on the method and conditions used in its preparation and/or the particle size distribution of the precursor (i.e., $\gamma\text{-Fe}_2\text{O}_3$ or Fe_3O_4 nanoparticles); the latter is particularly relevant in syntheses based on a size-induced phase transformation mechanism. Several synthetic routes for the preparation of $\varepsilon\text{-Fe}_2\text{O}_3$ have been reported. However, most of these yield $\gamma\text{-Fe}_2\text{O}_3$ and/or $\alpha\text{-Fe}_2\text{O}_3$ as impurities, the content of which significantly depends on the type of synthesis employed.³ $\varepsilon\text{-Fe}_2\text{O}_3$ nanoobjects can be prepared by direct decomposition using a suitable Fe-containing precursor and assisted by high-energy deposition techniques, sol–gel methods, a combination of reverse micelles and sol–gel methods, the microemulsion/sol–gel method, or vapor–liquid–solid mechanisms assisted by pulsed laser deposition (for a detailed overview of procedures for the synthesis of $\varepsilon\text{-Fe}_2\text{O}_3$, see Tucek et al.³). Several different Fe-containing compounds have been used as precursors in these syntheses, including $\text{Fe}_2\text{O}_3 \cdot 4\text{BeO}$, iron oxide aerosol, $6\text{Fe}_2(\text{SO}_4)_3 \cdot \text{Fe}_2\text{O}_3 \cdot n\text{H}_2\text{O}$, an aqueous mixture of $\text{K}_3\text{Fe}(\text{CN})_6$, NaClO , and KOH , $(\text{CaO}_{0.5}, \text{Na})_{0.5}\text{Fe}_2(\text{Si}, \text{Al})\text{O}_{10}(\text{OH})_2 \cdot n\text{H}_2\text{O}$, $\text{Pd}_{96}\text{Fe}_4$ alloy, iron(II) formate, a gaseous mixture of $\text{Fe}(\text{CO})_5$ and N_2O , $\text{Fe}(\text{NO}_3)_3$, FeSO_4 , $\text{Y}_3\text{Fe}_5\text{O}_{12}$, Fe_3O_4 , and $\gamma\text{-Fe}_2\text{O}_3$. In general, synthetic routes that use $\gamma\text{-Fe}_2\text{O}_3$ either as a precursor or as the last intermediate product yield the $\varepsilon\text{-Fe}_2\text{O}_3$ with the lowest portion of other Fe_2O_3 polymorphs. In addition, such synthetic procedures involve growth of $\gamma\text{-Fe}_2\text{O}_3$ precursor nanoparticles that, upon heat treatment, transform to $\varepsilon\text{-Fe}_2\text{O}_3$ at a given temperature when the size of a $\gamma\text{-Fe}_2\text{O}_3$ precursor nanoparticle reaches a certain threshold limit. The formation of $\varepsilon\text{-Fe}_2\text{O}_3$ requires a certain degree of agglomeration of the $\gamma\text{-Fe}_2\text{O}_3$ precursor nanoparticles, which is generally achieved through the

use of a supporting medium. In most cases, a silica matrix (a porous network formed from tetraethoxysilane (TEOS) and/or $\text{Si}(\text{C}_2\text{H}_5\text{O})_4$) is used, providing pores of a defined size that serve both as nucleation sites for the formation of $\varepsilon\text{-Fe}_2\text{O}_3$ nanoobjects and as size-restricted spaces that prevent excessive particle agglomeration. In addition, if Group IIA metal ions (e.g., Sr^{2+} and Ba^{2+} ions) are employed during the synthesis of $\varepsilon\text{-Fe}_2\text{O}_3/\text{SiO}_2$ nanocomposites, the portion of undesired Fe_2O_3 polymorphs (namely, $\alpha\text{-Fe}_2\text{O}_3$ and $\gamma\text{-Fe}_2\text{O}_3$) is significantly reduced.^{3,86,140,141} In addition, the presence of Group IIA metal ions in the reaction mixture promotes the growth of the product $\varepsilon\text{-Fe}_2\text{O}_3$ nanoobjects strengthening their stability against transformation to $\alpha\text{-Fe}_2\text{O}_3$ at a given reaction temperature and facilitating the production of nanoparticles with nanorod and/or nanowire structures.

So far, only a few studies have been focused on the effects of cation substitution on the structural and magnetic properties of $\varepsilon\text{-Fe}_2\text{O}_3$. To date, Ga^{3+} , Al^{3+} , and In^{3+} ions have been introduced into the crystal structure of $\varepsilon\text{-Fe}_2\text{O}_3$, replacing Fe^{3+} ions to various extents.^{3,93,142–144} Such cation substitution causes significant changes in the room- and low-temperature magnetic properties of $\varepsilon\text{-Fe}_2\text{O}_3$; the degree of cationic substitution also has profound effects on the average particle size and the particle size distribution of the product $\varepsilon\text{-Fe}_2\text{O}_3$ nanoobjects, although no simple relationship between the degree of substitution and the magnitude of these changes has yet been derived (the changes in the average particle size and particle size distribution happened in a rather random way on increasing the doping of non-iron cations). On the other hand, it was found that the morphology of cation-substituted $\varepsilon\text{-Fe}_2\text{O}_3$ nanoobjects was preserved no matter how high the substitution level was.

The purest samples of $\varepsilon\text{-Fe}_2\text{O}_3$ prepared to date were synthesized using a silica matrix to confine the growing nanoparticles and Group IIA metal ions to control the nanoparticles' size and morphology; samples prepared by this method have undetectable levels of other Fe_2O_3 polymorphs ($\gamma\text{-Fe}_2\text{O}_3$ and $\alpha\text{-Fe}_2\text{O}_3$).³ This protocol relies on the well-known $\gamma\text{-Fe}_2\text{O}_3 \rightarrow \varepsilon\text{-Fe}_2\text{O}_3 \rightarrow \alpha\text{-Fe}_2\text{O}_3$ phase transformation pathway; $\gamma\text{-Fe}_2\text{O}_3$ nanoparticles are initially produced in the pores of silica matrix by heat treatment of a suitable iron-containing precursor, grown by further heating, and finally transformed to $\varepsilon\text{-Fe}_2\text{O}_3$ nanoparticles (nanorods or nanowires) with a higher average size than the $\gamma\text{-Fe}_2\text{O}_3$ nanoparticles. This particle size-induced phase transformation mechanism that takes place inside the pores of the supporting matrix thus constitutes a controllable method for the preparation of high purity $\varepsilon\text{-Fe}_2\text{O}_3$ nanoobjects. In addition, the presence of a supporting matrix significantly increases the temperature at which the irreversible $\varepsilon\text{-Fe}_2\text{O}_3 \rightarrow \alpha\text{-Fe}_2\text{O}_3$ phase transformation occurs. It has been shown that if $\gamma\text{-Fe}_2\text{O}_3$ nanoparticles are not confined in a silica matrix but their agglomeration is suitably restricted, $\gamma\text{-Fe}_2\text{O}_3$ nanoparticles are converted to $\varepsilon\text{-Fe}_2\text{O}_3$ nanoparticles at temperatures of about 400 °C.³ Such unconfined $\varepsilon\text{-Fe}_2\text{O}_3$ nanoparticles are readily transformed to $\alpha\text{-Fe}_2\text{O}_3$ nanoparticles (whose average size is greater than that of the agglomerated $\varepsilon\text{-Fe}_2\text{O}_3$ nanoparticles) at temperatures between 400 and 1000 °C; the precise temperature at which this occurs is primarily dependent on the degree of particle aggregation and the average particle size. However, if the $\gamma\text{-Fe}_2\text{O}_3$ nanoparticles are imprisoned in the pores of silica matrix, the $\gamma\text{-Fe}_2\text{O}_3 \rightarrow \varepsilon\text{-Fe}_2\text{O}_3$ phase transformation occurs at relatively high temperatures (>1000 °C) (see Figure 6).³ The so-formed $\varepsilon\text{-Fe}_2\text{O}_3$ nanoparticles are stable up to 1400 °C, at which temperature the SiO_2 matrix decomposes and the

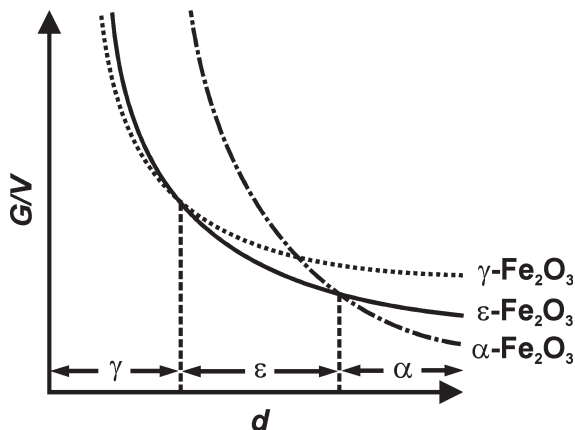


Figure 9. Stability of individual polymorphs of Fe_2O_3 based on the calculated dependence of the free energy per volume (G/V) on the size (d) of the iron(III) oxide nanoparticles of a particular polymorph (dependences derived under the conditions of $\eta_\alpha < \eta_\epsilon < \eta_\gamma$, $\sigma_\alpha > \sigma_\epsilon > \sigma_\gamma$ and $(\sigma_\epsilon - \sigma_\gamma)/(\eta_\epsilon - \eta_\gamma) > (\sigma_\epsilon - \sigma_\alpha)/(\eta_\epsilon - \eta_\alpha)$). Adapted with permission from Ohkoshi et al.¹⁴⁰ Copyright 2005 American Institute of Physics.

$\varepsilon\text{-Fe}_2\text{O}_3 \rightarrow \alpha\text{-Fe}_2\text{O}_3$ phase transformation occurs. The use of a supporting matrix thus increases the thermal stability of $\varepsilon\text{-Fe}_2\text{O}_3$.

In general, two factors have been found to play an essential role in determining which nanosized Fe_2O_3 polymorph will be formed from a given precursor and how it can subsequently be transformed into various iron(III) phases.^{3,121,140} These parameters include the free energy (G) per volume (V) of the different $i\text{-Fe}_2\text{O}_3$ phases ($i = \alpha, \beta, \gamma, \varepsilon$) and the energy barrier that must be overcome for the phase transformation to take place. The G/V ratio can be expressed as a function of the chemical potential (η) and the surface energy (σ), i.e., $G/V = \eta/v + 6\sigma/d$, where v is the molar volume and d denotes the size of a nanoparticle. Using this equation, it can be shown that $\varepsilon\text{-Fe}_2\text{O}_3$ can exist when the size of the Fe_2O_3 particle falls within an interval defined by $-6v(\sigma_\epsilon - \sigma_\gamma)/(\eta_\epsilon - \eta_\gamma) < d < -6v(\sigma_\epsilon - \sigma_\alpha)/(\eta_\epsilon - \eta_\alpha)$, satisfying conditions that (i) $\eta_\alpha < \eta_\epsilon < \eta_\gamma$, (ii) $\sigma_\alpha > \sigma_\epsilon > \sigma_\gamma$, and (iii) $(\sigma_\epsilon - \sigma_\gamma)/(\eta_\epsilon - \eta_\gamma) > (\sigma_\epsilon - \sigma_\alpha)/(\eta_\epsilon - \eta_\alpha)$.¹²¹ This implies that if nanoparticles of Fe_2O_3 grow large enough, the existence of $\varepsilon\text{-Fe}_2\text{O}_3$ is no longer favored (see Figure 9). In other words, reducing the sizes of the Fe_2O_3 particle increases the contribution of the surface (or interface) energy to G , which stabilizes $\varepsilon\text{-Fe}_2\text{O}_3$ in the nanoscaled size.

Recently, a successive $\gamma\text{-Fe}_2\text{O}_3 \rightarrow \varepsilon\text{-Fe}_2\text{O}_3 \rightarrow \beta\text{-Fe}_2\text{O}_3 \rightarrow \alpha\text{-Fe}_2\text{O}_3$ polymorphous transformation has been reported by Sakurai et al.⁵⁴ These authors used two precursors, FeSO_4 and $\text{Fe}(\text{C}_{10}\text{H}_9\text{CHO})$, each of which was impregnated into the pores of the SiO_2 matrix. Fe_2O_3 nanoparticles were then prepared by isothermal heating at temperatures above 900°C for 4 h followed by etching of the SiO_2 matrix. The particle size and crystal structure of the so-formed Fe_2O_3 was found to be dependent on the reaction temperature. Figure 10 shows how the phase composition of the Fe_2O_3 product varied with the preparation temperature when using $\text{Fe}(\text{C}_{10}\text{H}_9\text{CHO})$ as the precursor. Interestingly, the polymorphous transformation of $\varepsilon\text{-Fe}_2\text{O}_3$ to $\beta\text{-Fe}_2\text{O}_3$ was reported for the first time. The authors explained the successive polymorphous transformations as a consequence of a progressive increase in particle size as the temperature rose. All of the experiments were performed ex situ at a given constant temperature, and so it remains to be determined whether there is

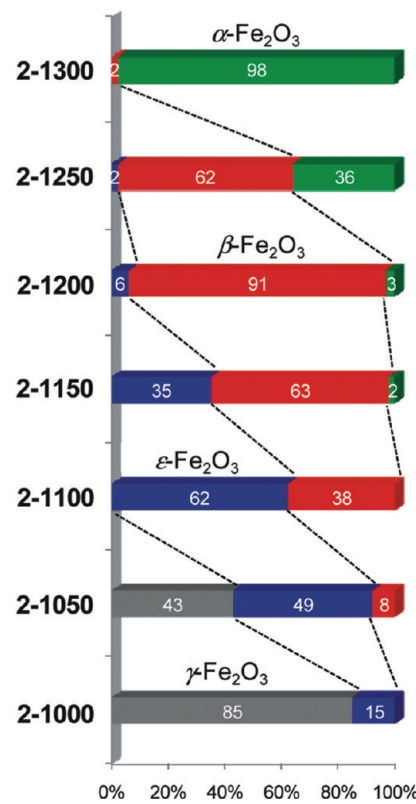


Figure 10. Contents of the four Fe_2O_3 phases obtained at different temperatures using $\text{Fe}(\text{C}_{10}\text{H}_9\text{CHO})$ as the precursor. Reprinted with permission from Sakurai et al.⁵⁴ Copyright 2009 American Chemical Society.

a continuous evolution in the particles' phase composition as the temperature increases.

The different forms of Fe_2O_3 may be formed successively or simultaneously during the experiments, depending on (i) the physical properties of the SiO_2 matrix, which change as the temperature rises (the glass transition temperature is about 1200°C); (ii) the extent to which the precursors are converted, which increases as the temperature rises; and (iii) the ability of the conversion gases (SO_3 , CO_2 , H_2O) to diffuse through the matrix. Therefore, the space restrictions imposed by the SiO_2 matrix can result in the preferential formation of $\gamma\text{-Fe}_2\text{O}_3$ and $\varepsilon\text{-Fe}_2\text{O}_3$ at temperatures below the glass transition temperature of the matrix, as discussed above. In our opinion, $\beta\text{-Fe}_2\text{O}_3$ observed at higher temperatures, when the SiO_2 matrix softens, is more likely to be formed directly from the precursor than via a polymorphous transformation of $\varepsilon\text{-Fe}_2\text{O}_3$. This means that $\beta\text{-Fe}_2\text{O}_3$ and $\varepsilon\text{-Fe}_2\text{O}_3$, which coexist between 1050 and 1250°C ,⁵⁴ may be formed simultaneously as a consequence of differences in the extent to which conversion gas is able to diffuse in different regions of the SiO_2 matrix. This question could be resolved by experiments using *in situ* high temperature X-ray powder diffraction and/or ^{57}Fe Mössbauer spectroscopy.

To date, only two mechanisms for the thermally induced polymorphous transformation of $\varepsilon\text{-Fe}_2\text{O}_3$ have been proposed. In most cases,^{119–121,123} $\varepsilon\text{-Fe}_2\text{O}_3$ was directly converted to $\alpha\text{-Fe}_2\text{O}_3$ once the reaction temperature became high enough to eliminate space restrictions and permit the agglomeration and sintering of ferric oxide particles. The second mechanism, reported by Sakurai et al.,⁵⁴ involves a sequential $\varepsilon\text{-Fe}_2\text{O}_3 \rightarrow \beta\text{-Fe}_2\text{O}_3 \rightarrow \alpha\text{-Fe}_2\text{O}_3$

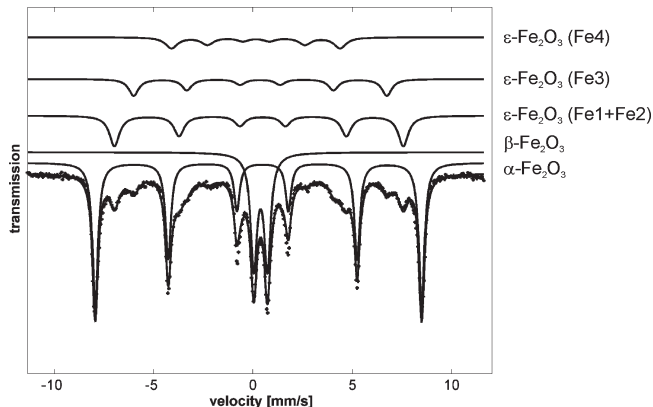


Figure 11. Room-temperature ^{57}Fe Mössbauer spectrum of a sample prepared by thermal conversion of $\text{Fe}(\text{SO}_4)_3 \cdot 5\text{H}_2\text{O}$ and its deconvolution to the spectral components corresponding to $\epsilon\text{-Fe}_2\text{O}_3$ (3 sextets), $\beta\text{-Fe}_2\text{O}_3$ (doublet), and $\alpha\text{-Fe}_2\text{O}_3$ (sextet).

polymorphous transformation. In our opinion, the $\epsilon\text{-Fe}_2\text{O}_3 \rightarrow \beta\text{-Fe}_2\text{O}_3$ phase transformation is rather improbable and probably reflects a misinterpretation of the experimental data; it is more likely that what was in fact observed by these authors was the simultaneous direct formation of $\beta\text{-Fe}_2\text{O}_3$ and $\epsilon\text{-Fe}_2\text{O}_3$ from the precursor.

5. SIMULTANEOUS VERSUS CONSEQUENT FORMATION OF IRON(III) OXIDE POLYMORPHS DURING THERMAL PROCESSES

Some of the reported conclusions about the formation of ferric oxide polymorphs are likely to be erroneous because the authors neglected to consider the possibility that under certain conditions, two different ferric oxide polymorphs might be formed simultaneously from the same precursor and subsequently be converted to $\alpha\text{-Fe}_2\text{O}_3$ by thermal processes. Thus, the simultaneous formation of two polymorphs can compete with their consequent structural transformation to the most thermally stable polymorph, $\alpha\text{-Fe}_2\text{O}_3$. The simultaneous formation of multiple polymorphs during the thermal decomposition of a single chemical compound is a relatively rare phenomenon in solid state chemistry and has only been confirmed to occur with a few precursors, including $\text{Fe}_2(\text{SO}_4)_3$, FeSO_4 , $\text{FeC}_2\text{O}_4 \cdot 2\text{H}_2\text{O}$, and $\text{Fe}_4[\text{Fe}(\text{CN})_6]_3$.^{53,130,131,145,146} Its occurrence is attributed to inhomogeneity in the reaction conditions within the sample. In the cases of $\text{Fe}_2(\text{SO}_4)_3$, FeSO_4 , and $\text{Fe}_4[\text{Fe}(\text{CN})_6]_3$, the inhomogeneity was found to be related to differences in the scope for the diffusion of a conversion gas from the surface and bulk of precursor particles. The phenomenon was first observed when it was noticed that the relative proportions of Fe_2O_3 polymorphs formed by heating specific precursors varied as a function of the precursor's particle size. While $\beta\text{-Fe}_2\text{O}_3$ was preferentially formed in the particles' surface layers, $\gamma\text{-Fe}_2\text{O}_3$ with a vacant structure and/or intermediate $\epsilon\text{-Fe}_2\text{O}_3$ were the primary decomposition products in the bulk of the particles, where the ability of the conversion gas to diffuse away was greatly reduced. It is worth mentioning that $\text{Fe}_2(\text{SO}_4)_3$ and/or FeSO_4 are the only precursors that can be used to form $\epsilon\text{-Fe}_2\text{O}_3$ in the absence of a supporting matrix, albeit as part of a mixture of Fe_2O_3 polymorphs rather than as a pure material. The deconvoluted Mössbauer spectrum of the products of the thermal decomposition of ferric sulfate, $\text{Fe}(\text{SO}_4)_3 \cdot 5\text{H}_2\text{O}$, at 590 °C is shown in Figure 11; the components corresponding to $\beta\text{-Fe}_2\text{O}_3$ and $\epsilon\text{-Fe}_2\text{O}_3$, which are formed simultaneously,

are highlighted along with that corresponding to $\alpha\text{-Fe}_2\text{O}_3$, which is formed by the transformation of the two initially formed ferric oxide polymorphs.

The effect of the thickness of the sample layer on the thermally induced oxidative decomposition of $\text{FeC}_2\text{O}_4 \cdot 2\text{H}_2\text{O}$ in air has been studied.¹⁴⁶ It was found that there was a critical sample layer thickness at a certain adjusted temperature below which it became possible for oxygen to efficiently access the entirety of the powdered sample; under such conditions, $\alpha\text{-Fe}_2\text{O}_3$ was the primary decomposition product. Above this critical layer thickness, the inability of oxygen to diffuse efficiently throughout the sample caused a time-limited increase in the sample temperature (exoeffect), after which the oxalate decomposed, yielding the vacant $\gamma\text{-Fe}_2\text{O}_3$ structure. The simultaneous formation of $\alpha\text{-Fe}_2\text{O}_3$ and $\gamma\text{-Fe}_2\text{O}_3$ during the thermally induced oxidative decomposition of $\text{FeC}_2\text{O}_4 \cdot 2\text{H}_2\text{O}$ at various temperatures¹⁴⁵ can therefore be attributed to differences in the diffusion conditions at the top and the bottom of the sample layer. This phenomenon has been also investigated using other iron-containing precursors, including iron(II) acetate dihydrate, iron(III) ferrocyanide, potassium ferrocyanide, and iron(III) oxalate hexahydrate,¹⁴⁶ all of which decompose into a single ferric oxide phase or mixtures of its polymorphs. Generally, $\alpha\text{-Fe}_2\text{O}_3$ and $\beta\text{-Fe}_2\text{O}_3$ were formed preferentially when a thin sample layer was heated, while the vacant $\gamma\text{-Fe}_2\text{O}_3$ structure and the intermediate $\epsilon\text{-Fe}_2\text{O}_3$ phase were observed when a thick sample layer was heated. This is illustrated by the example of the thermally induced oxidative decomposition of iron(II) acetate (see Figure 12): heat treatment of a thin precursor layer resulted in the formation of pure $\alpha\text{-Fe}_2\text{O}_3$ nanoparticles, while treatment of a thick layer afforded pure $\gamma\text{-Fe}_2\text{O}_3$ nanoparticles.¹⁴⁶ If the objective was to maximize the resulting powdered $\epsilon\text{-Fe}_2\text{O}_3$ content without using a supporting matrix, it would therefore make sense to combine the poor diffusion conditions encountered when using large precursor particles with the use of a thick layer of the ferric sulfate precursor during thermal conversion.

6. MECHANICALLY INDUCED POLYMORPHOUS TRANSFORMATIONS OF Fe_2O_3

Heat treatment is the most commonly used and experimentally convenient method of inducing the polymorphous transformations of iron(III) oxide. However, phase transformations can also be induced by milling, laser irradiation, or the application of high pressure to a sample. An “up-down” particle size-induced phase transformation of microcrystalline $\alpha\text{-Fe}_2\text{O}_3$ ($\sim 10\text{ }\mu\text{m}$) to nanocrystalline $\gamma\text{-Fe}_2\text{O}_3$ ($\sim 12\text{ nm}$) was achieved by hard mechanical grinding in an ethanol medium using a high-energy planetary ball mill.¹⁴⁷ Meillon et al.¹⁴⁸ reported that mechanical grinding of $\alpha\text{-Fe}_2\text{O}_3$ induced a direct phase transformation to $\gamma\text{-Fe}_2\text{O}_3$. Chernyshova et al. also found that mechanical treatment induced the $\alpha\text{-Fe}_2\text{O}_3$ -to- $\gamma\text{-Fe}_2\text{O}_3$ phase transformation and that the critical size for the dry $\alpha\text{-Fe}_2\text{O}_3$ nanoparticles in this process was $\sim 40\text{ nm}$.¹⁴⁹ Below this size, structural defects in the tetrahedral sites of the iron atoms at the surface of nanoparticles appeared to promote the gradual formation of $\gamma\text{-Fe}_2\text{O}_3$. This uncommon and thermodynamically disfavored structural transformation was explained by invoking a shearing mechanism based on the movement of oxygen planes in $\alpha\text{-Fe}_2\text{O}_3$ during milling, which was proposed to result in the formation of the vacant crystal structure.¹⁴⁸ Ferrimagnetic nanosized $\gamma\text{-Fe}_2\text{O}_3$, which is widely used in the production of magnetic materials, can be easily and inexpensively prepared on a large scale using this procedure.

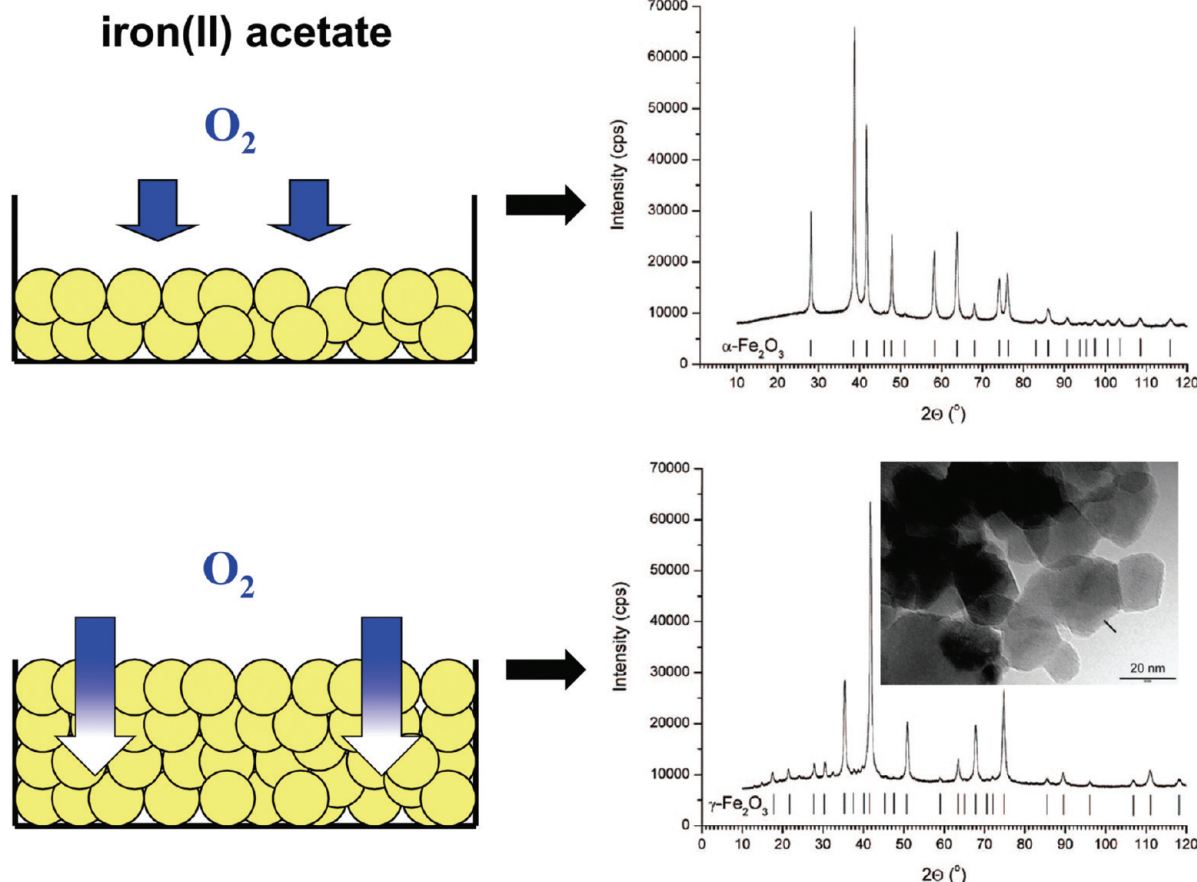


Figure 12. XRD patterns of α -Fe₂O₃ and γ -Fe₂O₃ samples prepared from iron(II) acetate at 245 °C using thin and thick layers of the precursor, respectively. The TEM image shows the perfect crystallinity and well-defined cubic morphology of γ -Fe₂O₃ nanoparticles. Adapted with permission from Hermanek et al.¹⁴⁶ Copyright 2008 American Chemical Society.

Table 2. Summary of the Phases Obtained by High-Pressure Treatment of α -Fe₂O₃

| pressure [GPa] | temperature [K] | structure | symmetry | space group | lattice constants [Å] | ref |
|----------------|-----------------|--|--------------|--------------|--------------------------------|-----|
| 30 | 2000 | perovskite | orthorhombic | Pbnm | $a = 4.90, b = 5.04, c = 7.15$ | 6 |
| 58 | 1400 | Rh ₂ O ₃ (II)-type | orthorhombic | Pbcn | $a = 6.67, b = 4.60, c = 4.94$ | 5 |
| 70 | 2500 | post-perovskite | orthorhombic | ^a | $a = 2.64, b = 6.39, c = 8.54$ | 6 |
| 96 | 2800 | perovskite | monoclinic | Cmcm | $a = 5.28, b = 6.39, c = 4.94$ | 6 |
| | | | | | $a = 2.64, b = 8.54, c = 6.39$ | 7 |

^a Not applicable.

In addition to the four conventional Fe₂O₃ polymorphs, the existence of “high-pressure” forms of Fe₂O₃, prepared by exposing samples of α -Fe₂O₃ to ultrahigh pressure, has been reported in several publications; see Table 2.^{5–9} Ito et al.⁵ used a multi-anvil apparatus equipped with sintered diamond anvils to induce successive transitions of α -Fe₂O₃ to the Rh₂O₃(II)-type Fe₂O₃ structure and then to an orthorhombic structure by increasing the pressure up to 58 GPa at 1400 K. Similarly, the high-pressure and high-temperature transitions of α -Fe₂O₃ to orthorhombic perovskite-type Fe₂O₃ structures were studied by Ono et al.⁶ These authors observed that the application of a pressure of 30 GPa and laser heating at 2000 K resulted in the formation of Fe₂O₃ with a perovskite-type structure (Pbnm). This first order phase transition was accompanied by a 3% change in the sample’s volume. When the pressure was increased to 70 GPa and the

temperature to 2500 K, other perovskite-like structures with both orthorhombic and monoclinic symmetry were observed. In this case, the first order phase transition to the so-called “post-perovskite” Fe₂O₃ phase was accompanied by a 7% change in the sample’s volume. A further increase in pressure (to 96 GPa) and temperature (to 2800 K) resulted in the conversion of the perovskite structure to a CaIrO₃-type structure with an orthorhombic symmetry (Cmcm space group, see Figure 13). The transformations were found to be reversible; the sample’s structure reverted back to that of α -Fe₂O₃ when the pressure was released. The phase diagram produced by Ono et al.⁶ is shown in Figure 14 (the phase boundaries are indicated by dashed lines). Since the temperature was estimated from the emissions of the heated sample, the uncertainty in the measurements was greater than that encountered when using the spectroradiometric method.

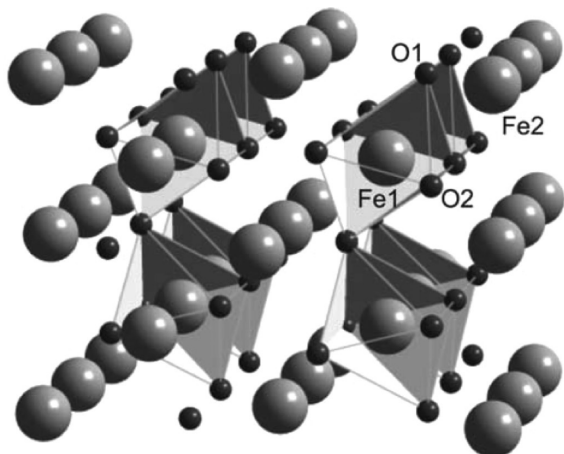


Figure 13. Refined CaIrO₃-type structure in the high-pressure Fe₂O₃ phase. Reprinted with permission from Ono and Ohishi.⁷ Copyright 2005 Elsevier.

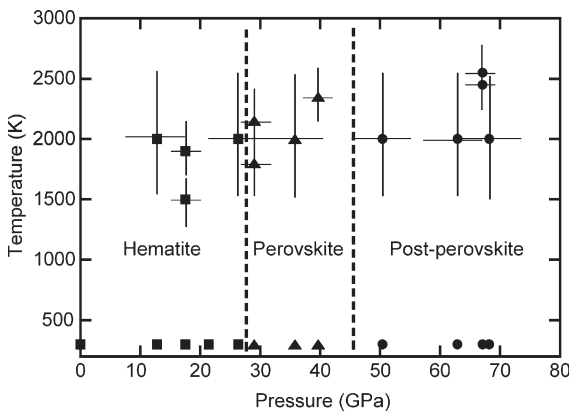


Figure 14. Phase diagram of the Fe₂O₃ phases formed at high pressure, as reported by Ono et al.⁶ Squares: α -Fe₂O₃; triangles: perovskite-type phase; circles: post-perovskite phase. Reprinted with permission from Ono et al.⁶ Copyright 2005 Elsevier.

In addition to the changes to the structure of Fe₂O₃, a pressure-induced electronic transition between high-spin and low-spin states of iron atoms was also detected.^{8,150,151}

High-pressure mechanical treatment has been used to induce the polymorphous transformation of γ -Fe₂O₃ to α -Fe₂O₃.^{152–157} The pressure threshold required to initiate the γ -Fe₂O₃-to- α -Fe₂O₃ phase transformation was found to be highly dependent on the particle size of the transformed γ -Fe₂O₃. Clark et al.¹⁵² confirmed that the transition pressure increased as the size of the γ -Fe₂O₃ nanocrystals decreased; specifically, 7 nm nanocrystals were transformed at 27 (± 2) GPa, 5 nm crystals at 34 (± 3) GPa, and 3 nm crystals at 37 (± 2) GPa. The increase in the transition pressure at small particle sizes was attributed to an increased contribution of the surface energy to the total energy. Wang and Saxena¹⁵⁴ studied the behavior of spherical nanocrystalline (25 nm) γ -Fe₂O₃ particles at pressures of up to 57.5 GPa. γ -Fe₂O₃ is initially transformed to the α -Fe₂O₃ phase at 13.5 GPa; the phase conversion is complete at 26.6 GPa. Further increases in the pressure resulted in the formation of the “high-pressure” perovskite structure described in the previous paragraph. While the “high-pressure” Fe₂O₃ structure reverted to

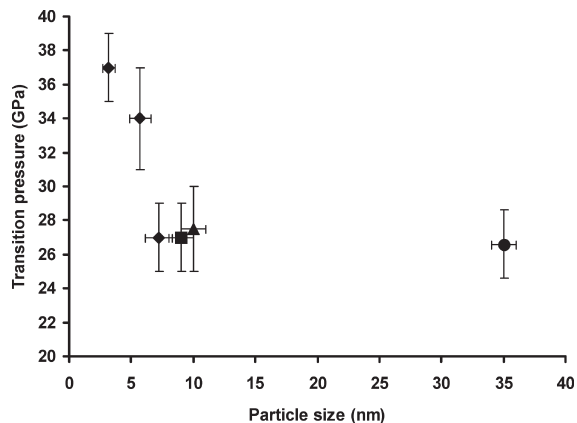


Figure 15. Variation of the transition pressure for the γ -Fe₂O₃-to- α -Fe₂O₃ phase transformation as a function of the size of the γ -Fe₂O₃ nanocrystals. Diamonds indicate data reported by Clark et al.,¹⁵² squares represent data reported by Jiang et al.,¹⁵⁵ triangles indicate data reported by Zhao et al.,¹⁵⁷ and circles represent data reported by Wang and Saxena.¹⁵⁴ Reprinted with permission from Clark et al.¹⁵² Copyright 2005 Institute of Physics Publishing.

α -Fe₂O₃ on pressure release, the γ -Fe₂O₃-to- α -Fe₂O₃ phase transformation was always irreversible, as expected. Kawakami et al.¹⁵³ conducted a very similar set of high-pressure experiments on γ -Fe₂O₃ and obtained results that were almost identical to those of Wang and Saxena.¹⁵⁴ These authors monitored changes in the direction of magnetization with respect to the direction of γ -rays during in situ high-pressure Mössbauer measurements. The angle between the incident γ -rays and the magnetization direction changed from being random to nearly parallel as the pressure increased. The variation of the transition pressure as a function of nanocrystal size for γ -Fe₂O₃ determined by different authors^{152,154,155,157} is shown in Figure 15.

Interestingly, only the mechanically activated polymorphous transformations of α -Fe₂O₃ and γ -Fe₂O₃ have been investigated to date. No systematic study on the mechanical treatment of the less common β -Fe₂O₃ and ε -Fe₂O₃ phases has yet been published. It would therefore be interesting to perform such a study and compare the mechanisms of the observed transformation to those encountered during thermal treatment.

7. ANALYTICAL TOOLS USED WHEN STUDYING THE POLYMORPHOUS TRANSFORMATIONS OF Fe₂O₃

It is necessary to use powerful analytical techniques to reliably discriminate between the different structural forms of Fe₂O₃ and to study the polymorphous transformations of Fe₂O₃. For routine work, conventional X-ray powder diffraction together with ⁵⁷Fe Mössbauer spectroscopy is usually sufficient for the identification of different polymorphs of Fe₂O₃. However, the use of alternative experimental methods including thermal analysis, microscopic techniques (transmission and scanning electron microscopy, atomic force microscopy), energy dispersive X-ray diffraction, magnetization measurements, the Brunauer–Emmett–Teller (BET) specific surface area technique, and especially in situ (XRD, Mössbauer) measurements can provide further important insights into the kinetics and mechanisms of the polymorphous transformations of Fe₂O₃.

XRD. Section 5 discussed processes in which two different Fe₂O₃ polymorphs were simultaneously formed and transformed

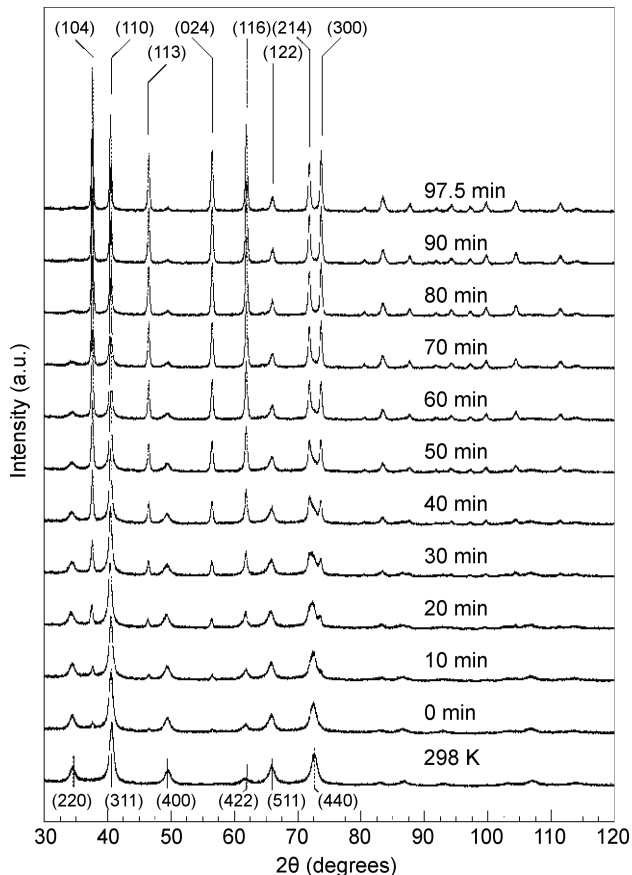


Figure 16. Structural evolution of a γ - Fe_2O_3 sample during the γ - Fe_2O_3 -to- α - Fe_2O_3 phase transformation at 723 K. The lower and higher indices denote γ - Fe_2O_3 and α - Fe_2O_3 , respectively. The shift due to temperature between 298 and 723 K on the XRD patterns was detected but is not visible in this figure. Reprinted with permission from Belin et al.¹¹¹ Copyright 2007 Elsevier.

to other ferric oxide polymorphs during heat treatment. The mechanical treatments described in Section 6 led to reversible polymorphous transformations of Fe_2O_3 . In all of these cases, the ability to acquire measurements *in situ* was particularly useful because it enables the direct monitoring of changes in the sample's crystal structure, crystallinity, and magnetism under the current physical conditions and can be used to monitor the kinetics of a polymorphous transformation. When studying high-temperature processes, *in situ* techniques have the advantage that their results are not affected by cooling processes or by any need to manipulate and store the samples between the heat treatment and its *ex situ* analysis.

In situ X-ray powder diffraction has been used to study the polymorphous transitions of Fe_2O_3 at high temperatures (γ - $\text{Fe}_2\text{O}_3 \rightarrow \alpha$ - Fe_2O_3 ,^{7,102,111,158} β - $\text{Fe}_2\text{O}_3 \rightarrow \gamma$ - Fe_2O_3 (ref 56)) and/or pressures.^{5,7} In special cases, *in situ* XRD using high-intensity synchrotron radiation has been employed;^{6,7,111,159} for example, this method was used to monitor the evolution of a γ - Fe_2O_3 sample at 723 K (see Figure 16).¹¹¹ These measurements were used to demonstrate the particle size-induced polymorphous transformation of γ - Fe_2O_3 to α - Fe_2O_3 by analysis of the sizes of the coherent domains within the sample (see Figure 2). Similarly, Ono et al.⁶ were able to distinguish between the GdFeO_3 orthorhombic perovskite-type structure and the

Rh_2O_3 -type structure when studying Fe_2O_3 samples under high pressures. When the temperature was raised above 1200 °C and an ultrahigh pressure of 96 GPa was applied, the Rh_2O_3 -type structure of Fe_2O_3 was converted to a CaIrO_3 -type structure with orthorhombic symmetry.⁷ In this case, the *in situ* X-ray synchrotron observations alone made it possible to establish the CaIrO_3 -type structure of the high-pressure ferric oxide phase (see Figure 13). Interestingly, no *in situ* high-temperature ^{57}Fe Mössbauer spectroscopy study of the polymorphous transformations of Fe_2O_3 has yet been reported. This is a shame; the combination of *in situ* X-ray powder diffraction and *in situ* ^{57}Fe Mössbauer spectroscopy would provide practically complete information on the sample's phase composition and would make it possible to perform quantitative measurements during the polymorphous transformations of Fe_2O_3 .

Mössbauer Spectroscopy. ^{57}Fe Mössbauer spectroscopy carried out at low temperatures in an external magnetic field is a particularly effective method for distinguishing between the different Fe_2O_3 polymorphs on the basis of their (nano)cocrystallinity. The power of Mössbauer spectroscopy can be demonstrated by its ability to unambiguously discriminate between nanocrystalline γ - Fe_2O_3 (see Figure 11) and amorphous Fe_2O_3 . These two ferric oxide phases exhibit very broad diffraction lines in their XRD patterns but have very different low-temperature/in-field Mössbauer spectra (see Figure 17).¹⁰

In addition to the key XRD and/or Mössbauer measurements, authors studying the polymorphous transformations of Fe_2O_3 have used a range of other supporting experimental techniques, including thermal analysis (TA),^{114,117,160} atomic force microscopy (AFM),^{103,127} transmission electron microscopy (TEM),^{110,54} energy dispersive X-ray diffraction (EDXRD),¹¹⁰ (micro-) Raman spectroscopy,^{126,139,154} and Fourier transform infrared spectroscopy (FTIR).^{109,126,149,161}

Thermal Analysis. Thermal analysis is an *in situ* technique in that it involves monitoring the thermal behavior of a sample during heat treatment. While polymorphous transformations are not expected to involve any changes in sample weight (and thus cannot be monitored by TGA), they do involve an exothermic event that can be observed by DSC (DTA): heat is evolved when a less stable crystal structure is converted to a more stable form. Exothermal peaks of this kind were observed between 440 and 550 °C in a DTA study of nanostructured γ - Fe_2O_3 samples by Ye et al.^{114,160} These workers confirmed that the peak did not reappear when the same sample was resubjected to DTA and therefore suggested that it is associated with an irreversible γ - Fe_2O_3 -to- α - Fe_2O_3 phase transformation. On the basis of the position of the exothermal peak in the DTA curve, Zhang et al.¹⁰⁵ determined that a nanostructured sample of γ - Fe_2O_3 doped with Y_2O_3 underwent the γ - Fe_2O_3 -to- α - Fe_2O_3 phase transformation at 725 °C, illustrating the enhanced thermal stability afforded by doping. DTA/TGA measurements were performed on γ - Fe_2O_3 nanoparticles coated with amorphous SiO_2 by Ichiyangi and Kimishima.¹⁶² A broad exothermal peak was observed at around 900 K on the DTA curve, indicating the γ - Fe_2O_3 -to- α - Fe_2O_3 phase conversion within the SiO_2 matrix to be relatively slow. In contrast to the isothermal conditions typically encountered when heating a sample in an external furnace, thermal analyses are generally carried out under dynamic heating conditions with a uniform rate of temperature increase. Therefore, the transformation temperatures determined by thermal analysis are higher than those measured in *ex situ* experiments (e.g., those performed in an external furnace).

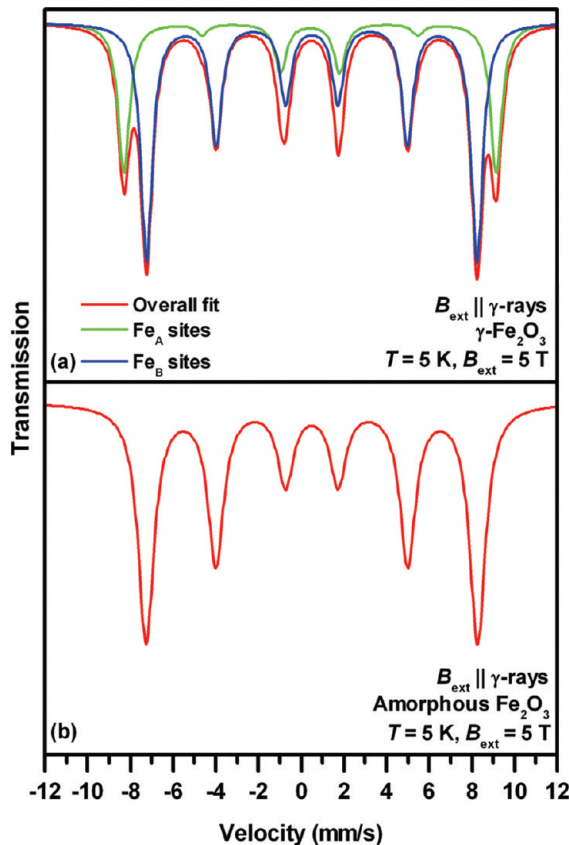


Figure 17. Modeled in-field low-temperature Mössbauer spectra of (a) nanocrystalline $\gamma\text{-Fe}_2\text{O}_3$ and (b) amorphous Fe_2O_3 .

Microscopy Techniques. TEM is a powerful tool for monitoring the evolution of particle size and morphology during the polymorphous transitions of Fe_2O_3 . TEM observations were used to confirm that there is a critical size that $\gamma\text{-Fe}_2\text{O}_3$ nanoparticles must exceed before undergoing a structural transformation to $\alpha\text{-Fe}_2\text{O}_3$.¹⁰⁵ TEM images also made it possible to determine and compare the particle sizes and morphologies of all four Fe_2O_3 polymorphs in the course of their successive thermally induced transformations within a mesoporous SiO_2 matrix (see Figure 18) and have been used to determine the threshold sizes for the individual structural transitions of Fe_2O_3 .⁵⁴ It should be noted that care is necessary when using high-intensity electron irradiation in TEM because it can induce undesirable in situ crystallization and/or polymorphous transitions in Fe_2O_3 . Similarly, the exposure of $\gamma\text{-Fe}_2\text{O}_3$ nanoparticles^{163,164} and/or nanowires¹⁶⁵ to a laser beam during the acquisition of their Raman spectra has been shown to promote their transformation to $\alpha\text{-Fe}_2\text{O}_3$.

Spectroscopic Techniques. (Micro-) Raman and FTIR spectroscopies have been used as supporting techniques in the characterization of precursors and/or matrices related to the syntheses of ferric oxide samples, as well as for assessing sample purity. Raman spectroscopy has also been used in the analysis of $\gamma\text{-Fe}_2\text{O}_3$ phase transformations, particularly with samples for which X-ray diffraction provides only poor information.¹²⁶

In conclusion, the in situ analytical approaches (XRD, Mössbauer spectroscopy, usage of synchrotron radiation) provide the most reliable and detailed information on the mechanisms of the polymorphous transformations of Fe_2O_3 under arbitrary physical

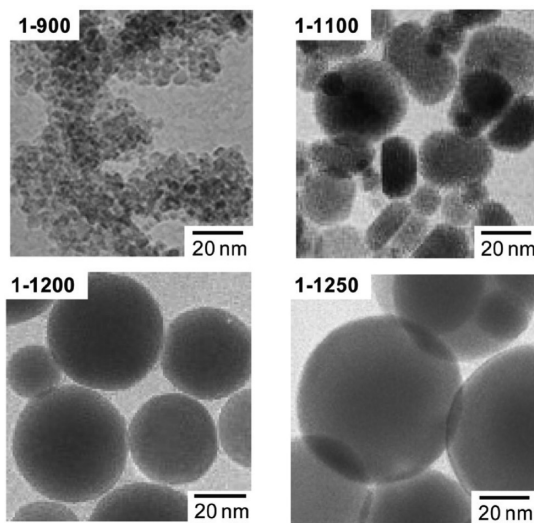


Figure 18. TEM images of Fe_2O_3 samples prepared by Sakurai et al.⁵⁴ demonstrating successive particle size-induced polymorphous transformations within the SiO_2 matrix. Legend: 1-900: $\gamma\text{-Fe}_2\text{O}_3$; 1-1100: $\varepsilon\text{-Fe}_2\text{O}_3$; 1-1200: $\beta\text{-Fe}_2\text{O}_3$; 1-1250: $\alpha\text{-Fe}_2\text{O}_3$. Reprinted with permission from Sakurai et al.⁵⁴ Copyright 2009 American Chemical Society.

conditions. Low-temperature and in-field Mössbauer spectroscopy has proven to be the most useful technique for distinguishing between the various polymorphs of Fe_2O_3 , without regard for their nanocrystallinity, and for identifying amorphous Fe_2O_3 .

8. SUMMARY AND OUTLOOK

One of the most important goals in the study of iron's solid state chemistry, from both basic and applied perspectives, is to understand the mechanisms and kinetics of the polymorphous transformations of iron(III) oxides and to be able to use that understanding to control these processes. This is largely because the different polymorphs have many unique properties and a wide range of potential applications. Notably, hematite ($\alpha\text{-Fe}_2\text{O}_3$) can be used in solar cells for the photocatalytic splitting of water, nanomaghemit ($\gamma\text{-Fe}_2\text{O}_3$) is used extensively in various medicinal fields (as a magnetic resonance imaging contrast agent, in magnetic drug delivery, and in hyperthermia-based anticancer therapy), $\varepsilon\text{-Fe}_2\text{O}_3$ exhibits giant room-temperature coercivity and is therefore useful in advanced magnetic applications, and the rare $\beta\text{-Fe}_2\text{O}_3$ phase has an unusual and highly interesting hollow structure. The study and practical use of these species requires that they are available as single phases that are not contaminated with any of the other polymorphs. However, most procedures for their synthesis involve high-temperature treatment, which induces diverse polymorphous transitions of metastable Fe_2O_3 species. In this review, we sought to highlight the dependence of the mechanism and kinetics of polymorphous transitions on a range of internal factors, including the polymorph structure, particle size, particle morphology, surface coating, particle aggregation, and embedding of particles in a matrix. The key external parameters include the transformation temperature, atmosphere, and pressure. A full understanding of the roles of all of these parameters is required to control the polymorphous transitions so as to produce pure single phases.

We have also sought to highlight some controversial issues related to the polymorphous transformations of iron(III) oxides. The most significant of these is the question of whether it is possible for multiple polymorphs to be formed simultaneously during the thermal conversion of iron-containing precursors and the subsequent polymorphous transitions of the so-formed iron(III) oxides. We believe that the observation of these simultaneous processes has led to some misinterpretations, such as the suggestion that the following sequence of polymorphous transformations may occur under certain circumstances: $\gamma\text{-Fe}_2\text{O}_3 \rightarrow \varepsilon\text{-Fe}_2\text{O}_3 \rightarrow \beta\text{-Fe}_2\text{O}_3 \rightarrow \alpha\text{-Fe}_2\text{O}_3$.¹⁰⁴ Thermodynamically, this seems highly improbable. Our experience with thermal decomposition suggests that, instead, the primary products in this process are probably $\gamma\text{-Fe}_2\text{O}_3$ and $\beta\text{-Fe}_2\text{O}_3$, which form simultaneously in different regions of the sample due to the inhomogeneities created by the use of a thick sample layer and differences in the sizes of the precursor particles. Additional studies will be needed to assess the viability of the proposed $\varepsilon\text{-Fe}_2\text{O}_3$ -to- $\beta\text{-Fe}_2\text{O}_3$ polymorphous transformation. The development of methods for the kinetic control of the transformation of $\gamma\text{-Fe}_2\text{O}_3 \rightarrow \varepsilon\text{-Fe}_2\text{O}_3$ is another challenge for the community; a practical method for achieving this transformation could be used in the large-scale synthesis of the $\varepsilon\text{-Fe}_2\text{O}_3$ nanophase, which has very useful magnetic properties. The effects of particle morphologies and the way they change during polymorphous transitions are still poorly understood. It would be particularly interesting to study these effects in the hollow $\beta\text{-Fe}_2\text{O}_3$ structure; if this species could be thermally converted to magnetic $\gamma\text{-Fe}_2\text{O}_3$ particles in a way that preserved its remarkable morphology, the resulting hollow $\gamma\text{-Fe}_2\text{O}_3$ nanoparticles would be excellent magnetic sorbents as well as suitable materials for targeted drug delivery. It has been shown that pressure-induced polymorphous transformations can generate a number of interesting high-pressure structures that are reversibly converted back to $\alpha\text{-Fe}_2\text{O}_3$ when the pressure is released. It would be very interesting if these high-pressure structures could be formed and then irreversibly stabilized using methods that exploit other sources of energy. Much remains to be learned about the pressure-induced transitions of polymorphs other than $\alpha\text{-Fe}_2\text{O}_3$. It is possible that the pressure-induced transformations of $\gamma\text{-Fe}_2\text{O}_3$, $\varepsilon\text{-Fe}_2\text{O}_3$, and $\beta\text{-Fe}_2\text{O}_3$ might give rise to new polymorphs. At low pressures, some of these transformations may be irreversible, as in the case of the irreversible conversion of $\alpha\text{-Fe}_2\text{O}_3$ to $\gamma\text{-Fe}_2\text{O}_3$ by low-pressure grinding. This ability to promote thermodynamically unfavorable transitions by the use of mechanical force deserves considerable study in the future.

AUTHOR INFORMATION

Corresponding Author

*Tel.: +420585634947. Fax: +420585634958. E-mail: zboril@prfnw.upol.cz.

ACKNOWLEDGMENT

This work was supported by the Operational Program Research and Development for Innovations – European Social Fund (CZ.1.05/2.1.00/03.0058), grants from the Ministry of Education of the Czech Republic (1M6198959201 and MSM6198959218), and a grant from the Academy of Sciences of the Czech Republic (KAN115600801).

REFERENCES

- (1) Cornel, R. M.; Schwertmann, U. *The Iron Oxides. Structure, Properties, Reactions and Uses*; Wiley-VCH: Weinheim, Germany, 2003.
- (2) Zboril, R.; Mashlan, M.; Petridis, D. *Chem. Mater.* **2002**, *14*, 969.
- (3) Tucek, J.; Zboril, R.; Namai, A.; Ohkoshi, S. *Chem. Mater.* **2010**, *22*, 6483.
- (4) Mahmoudi, M.; Stroeve, P.; Milani, A. S.; Arbab, A. S. *Superparamagnetic Iron Oxide Nanoparticles: Synthesis, Surface Engineering, Cytotoxicity & Biomedical Applications*; Nova Science Pub Inc.: U.K., 2011.
- (5) Ito, E.; Fukui, H.; Katsura, T.; Yamazaki, D.; Yoshino, T.; Alizawa, Y.; Kubo, A.; Yokoshi, S.; Kawabe, K.; Zhai, S. M.; Shatzkiy, A.; Okube, M.; Nozawa, A.; Funakoshi, K. *I. Am. Mineral.* **2009**, *94*, 205.
- (6) Ono, S.; Kikegawa, T.; Ohishi, Y. *J. Phys. Chem. Solids* **2004**, *65*, 1527.
- (7) Ono, S.; Ohishi, Y. *J. Phys. Chem. Solids* **2005**, *66*, 1714.
- (8) Badro, J.; Fiquet, G.; Struzhkin, V. V.; Somayazulu, M.; Mao, H. K.; Shen, G.; Le Bihan, T. *Phys. Rev. Lett.* **2002**, *89*, 205504.
- (9) Liu, H.; Caldwell, W. A.; Benedetti, L. R.; Panero, W.; Jeanloz, R. *Phys. Chem. Miner.* **2003**, *30*, 582.
- (10) Machala, L.; Zboril, R.; Gedanken, A. *J. Phys. Chem. B* **2007**, *111*, 4003.
- (11) Prucek, R.; Hermanek, M.; Zboril, R. *Appl. Catal., A* **2009**, *366*, 325.
- (12) Hermanek, M.; Zboril, R.; Medrik, I.; Pechousek, J.; Gregor, C. *J. Am. Chem. Soc.* **2007**, *129*, 10929.
- (13) Yusuf, S. M.; Mukadam, M. D.; De Teresa, J. M.; Ibarra, M. R.; Kohlbrecher, J.; Heinemann, A.; Wiedenmann, A. *Physica B* **2010**, *405*, 1202.
- (14) Tucek, J.; Zboril, R.; Petridis, D. *J. Nanosci. Nanotechnol.* **2006**, *6*, 926.
- (15) Morin, F. *J. Phys. Rev.* **1950**, *78*, 819.
- (16) Artman, J. O.; Murphy, J. C.; Foner, S. *Phys. Rev.* **1965**, *138*, A912.
- (17) Vandenberghe, R. E.; De Grave, E.; Landuydt, C.; Bowen, L. H. *Hyperfine Interact.* **1990**, *53*, 175.
- (18) Morrish, A. H. *Canted Antiferromagnetism: Hematite*; World Scientific Publishing Company: Singapore, 1994.
- (19) Suber, L.; Imperatori, P.; Mari, A.; Marchegiani, G.; Mansilla, M. V.; Fiorani, D.; Plunkett, W. R.; Rinaldi, D.; Cannas, C.; Ennas, G.; Peddis, D. *Phys. Chem. Chem. Phys.* **2010**, *12*, 6984.
- (20) Darezereshki, E. *Mater. Lett.* **2011**, *65*, 642.
- (21) Pailhe, N.; Wattiaux, A.; Gaudon, M.; Demourgues, A. *J. Solid State Chem.* **2008**, *181*, 2697.
- (22) Robinson, P.; Harrison, R. J.; McEnroe, S. A.; Hargraves, R. B. *Nature* **2002**, *418*, 517.
- (23) Le Formal, F.; Gratzel, M.; Sivula, K. *Adv. Funct. Mater.* **2010**, *20*, 1099.
- (24) Frydrych, J.; Machala, L.; Hermanek, M.; Medrik, I.; Mashlan, M.; Tucek, J.; Pechousek, J.; Sharma, V. K. *Thin Solid Films* **2010**, *518*, 5916.
- (25) Memar, A.; Daud, W. R. W.; Hosseini, S.; Eftekhar, E.; Minggu, L. *J. Sol. Energy* **2010**, *84*, 1538.
- (26) Wei, Q.; Zhang, Z. J.; Li, Z. C.; Zhou, Q.; Zhu, Y. *J. Phys. D: Appl. Phys.* **2008**, *41*, 202002.
- (27) Kleiman-Shwarscstein, A.; Hu, Y. S.; Forman, A. J.; Stucky, G. D.; McFarland, E. W. *J. Phys. Chem. C* **2008**, *112*, 15900.
- (28) Gondal, M. A.; Hameed, A.; Yamani, Z. H. *Chem. Phys. Lett.* **2004**, *385*, 111.
- (29) Souza, F. L.; Lopes, K. P.; Nascente, P. A. P.; Leite, E. R. *Sol. Energy Mater. Sol. Cells* **2009**, *93*, 362.
- (30) Hahn, N. T.; Mullins, C. B. *Chem. Mater.* **2010**, *22*, 6474.
- (31) Jang, J. S.; Yoon, K. Y.; Xiao, X. Y.; Fan, F. R. F.; Bard, A. J. *Chem. Mater.* **2009**, *21*, 4803.
- (32) Tahir, A. A.; Wijayanta, K. G. U.; Saremi-Yarahmadi, S.; Mazhar, M.; McKee, V. *Chem. Mater.* **2009**, *21*, 3763.
- (33) Hu, Y. S.; Kleiman-Shwarscstein, A.; Forman, A. J.; Hazen, D.; Park, J. N.; McFarland, E. W. *Chem. Mater.* **2008**, *20*, 3803.
- (34) Boumaza, S.; Boudjemaa, A.; Omeiri, S.; Bouarab, R.; Bouguelia, A.; Trari, M. *Sol. Energy* **2010**, *84*, 715.

- (35) Rettig, F.; Moos, R. *Sens. Actuators, B* **2010**, *145*, 685.
- (36) Chen, H. M.; Zhao, Y. Q.; Yang, M. Q.; He, J. H.; Chu, P. K.; Zhang, J.; Wu, S. H. *Anal. Chim. Acta* **2010**, *659*, 266.
- (37) Wu, Z. C.; Yu, K.; Zhang, S. D.; Xie, Y. *J. Phys. Chem. C* **2008**, *112*, 11307.
- (38) Tan, O. K.; Cao, W.; Zhu, W.; Chai, J. W.; Pan, J. S. *Sens. Actuators, B* **2003**, *93*, 396.
- (39) Chen, J.; Xu, L. N.; Li, W. Y.; Gou, X. L. *Adv. Mater.* **2005**, *17*, 582.
- (40) Huo, L. H.; Li, W.; Lu, L. H.; Cui, H. N.; Xi, S. Q.; Wang, J.; Zhao, B.; Shen, Y. C.; Lu, Z. H. *Chem. Mater.* **2000**, *12*, 790.
- (41) Prucek, R.; Hermanek, M.; Zboril, R. *Appl. Catal., A* **2009**, *366*, 325.
- (42) Wang, D. Y.; Liu, Z. Q.; Liu, F. G.; Zhang, X. T.; Cao, Y.; Yu, J. F.; Wu, T. H.; Bai, Y. B.; Li, T. J.; Tang, X. Y. *React. Kinet. Catal. Lett.* **1998**, *65*, 233.
- (43) Zhang, W.; Chen, J.; Wang, X.; Qi, H. L.; Peng, K. S. *Appl. Organomet. Chem.* **2009**, *23*, 200.
- (44) Huang, C. L.; Zhang, H. Y.; Sun, Z. Y.; Liu, Z. M. *Science China-Chemistry* **2010**, *53*, 1502.
- (45) Hermanek, M.; Zboril, R.; Medrik, I.; Pechousek, J.; Gregor, C. *J. Am. Chem. Soc.* **2007**, *129*, 10929.
- (46) Wang, G. H.; Li, W. C.; Jia, K. M.; Spliethoff, B.; Schuth, F.; Lu, A. H. *Appl. Catal., A* **2009**, *364*, 42.
- (47) Kahlich, M. J.; Gasteiger, H. A.; Behm, R. J. *J. Catal.* **1999**, *182*, 430.
- (48) Zhong, Z.; Ho, J.; Teo, J.; Shen, S.; Gedanken, A. *Chem. Mater.* **2007**, *19*, 4776.
- (49) Khoudakov, M.; Gupta, M. C.; Deevi, S. *Appl. Catal., A* **2005**, *291*, 151.
- (50) Kletetschka, G.; Wasilewski, P. J.; Taylor, P. T. *Tectonophysics* **2002**, *347*, 167.
- (51) McEnroe, S. A.; Carter-Stiglitz, B.; Harrison, R. J.; Robinson, P.; Fabian, K.; McCammon, C. *Nat. Nanotechnol.* **2007**, *2*, 631.
- (52) Zboril, R.; Mashlan, M.; Krausova, D.; Pikal, P. *Hyperfine Interact.* **1999**, *121*, 497.
- (53) Zboril, R.; Mashlan, M.; Machala, L.; Bezdicka, P. In *Material Research in Atomic Scale by Mossbauer Spectroscopy*; Mashlan, M., Miglierini, M., Schaaf, P., Eds.; Springer: Dordrecht, The Netherlands, 2003; Vol. 94, p 21.
- (54) Sakurai, S.; Namai, A.; Hashimoto, K.; Ohkoshi, S. *J. Am. Chem. Soc.* **2009**, *131*, 18299.
- (55) Mills, S. J.; Madsen, I. C.; Grey, I. E.; Birch, W. D. *Can. Mineral.* **2009**, *47*, 683.
- (56) Lee, C. W.; Lee, K. W.; Lee, J. S. *Mater. Lett.* **2008**, *62*, 561.
- (57) Hrbac, J.; Halouzka, V.; Zboril, R.; Papadopoulos, K.; Triantis, T. *Electroanal.* **2007**, *19*, 1850.
- (58) Lee, C. W.; Lee, K. W.; Lee, J. S. *Mater. Lett.* **2008**, *62*, 2664.
- (59) Zboril, R.; Mashlan, M.; Petridis, D.; Krausova, D.; Pikal, P. *Hyperfine Interact.* **2002**, *139*, 437.
- (60) Braun, P. B. *Nature (London)* **1952**, *179*, 1123.
- (61) Oosterhout, G. W.; Rooymans, C. J. M. *Nature (London)* **1958**, *181*, 44.
- (62) Morales, M. P.; Pecharroman, C.; Gonzalez-Carreno, T.; Serna, S. J. *J. Solid State Chem.* **1994**, *108*, 158.
- (63) Shafi, K. V. P. M.; Ulman, A.; Dyal, A.; Yan, X. Z.; Yang, N. L.; Estournes, C.; Fourches, L.; Wattiaux, A.; White, H.; Rafailovich, M. *Chem. Mater.* **2002**, *14*, 1778.
- (64) Kelm, K.; Mader, W. Z. *Naturforsch. B* **2006**, *61*, 665.
- (65) Jorgensen, J. E.; Mosegaard, L.; Thomsen, L. E.; Jensen, T. R.; Hanson, J. C. *J. Solid State Chem.* **2007**, *180*, 180.
- (66) Mørup, S.; Bødker, F.; Hendriksen, P. V.; Linderoth, S. *Phys. Rev. B* **1995**, *52*, 287.
- (67) Mørup, S.; Oxborrow, C. A.; Hendriksen, P. V.; Pedersen, M. S.; Hanson, M.; Johansson, C. *J. Magn. Magn. Mater.* **1995**, *409*, 140.
- (68) Tronc, E.; Jolivet, J. P.; Livage, J. *Hyperfine Interact.* **1990**, *54*, 737.
- (69) Dormann, J. L.; Fiorani, D.; Tronc, E. In *Advances in Chemical Physics*; Prigogine, I., Rice, S. A., Eds.; John Wiley: New York, 1997; Vol. 98, p 283.
- (70) Tronc, E.; Ezzir, A.; Cherkaoui, R.; Chanéac, C.; Nogues, M.; Kachkachi, H.; Fiorani, D.; Testa, A. M.; Grenache, J. M.; Jolivet, J. P. *J. Magn. Magn. Mater.* **2000**, *221*, 63.
- (71) Fiorani, D.; Dormann, J. L.; Cherkaoui, R.; Tronc, E.; Lucari, F.; D’Orazio, F.; Spinu, L.; Nogues, M.; Garcia, A.; Testa, A. M. *J. Magn. Magn. Mater.* **2000**, *196*, 143.
- (72) Dormann, J. L.; Cherkaoui, R.; Spinu, L.; Nogues, M.; Lucari, F.; D’Orazio, F.; Fiorani, D.; Garcia, A.; Tronc, E.; Jolivet, J. P. *J. Magn. Magn. Mater.* **1998**, *187*, L139.
- (73) Knobel, M.; Nunes, W. C.; Socolovsky, L. M.; De Biasi, E.; Vargas, J. M.; Denardin, J. C. *J. Nanosci. Nanotechnol.* **2008**, *8*, 2836–2857.
- (74) Sun, S. H. *Adv. Mater.* **2006**, *18*, 393–403.
- (75) Häfeli, U.; Schütt, W.; Teller, J.; Zboraski, M. *Scientific and Clinical Applications of Magnetic Carriers*; Plenum Press: New York, 1997.
- (76) Safarik, I.; Safarikova, M. *Monatsh. Chem.* **2002**, *133*, 737.
- (77) Pankhurst, Q. A.; Connolly, J.; Jones, S. K.; Dobson, J. *J. Phys. D: Appl. Phys.* **2003**, *36*, R167.
- (78) Gupta, A. K.; Gupta, M. *Biomaterials* **2005**, *26*, 3995.
- (79) Tartaj, P.; Morales, M. P.; Veintemillas-Verdaguer, S.; Gonzalez-Carreño, T.; Serna, C. *J. Phys. D: Appl. Phys.* **2003**, *36*, R182.
- (80) Berry, C. C.; Curtis, A. S. G. *J. Phys. D: Appl. Phys.* **2003**, *36*, R198.
- (81) Lu, A. H.; Salabas, E. L.; Schuth, F. *Angew. Chem., Int. Ed.* **2007**, *46*, 1222–1244.
- (82) Mornet, S.; Vasseur, S.; Grasset, F.; Duguet, E. *J. Mater. Chem.* **2004**, *14*, 2161–2175.
- (83) Tronc, E.; Chaneac, C.; Jolivet, J. P. *J. Solid State Chem.* **1998**, *139*, 93.
- (84) Gich, M.; Frontera, C.; Roig, A.; Taboada, E.; Molins, E.; Rechenberg, H. R.; Ardisson, J. D.; Macedo, W. A. A.; Ritter, C.; Hardy, V.; Sort, J.; Skumryev, V.; Nogues, J. *Chem. Mater.* **2006**, *18*, 3889.
- (85) Tseng, Y.-C.; Souza-Neto, N. M.; Haskel, D.; Gich, M.; Frontera, C.; Roig, A.; Van Veenendaal, M.; Nogues, J. *Phys. Rev. B* **2009**, *79*, 094404.
- (86) Jin, J.; Ohkoshi, S.; Hashimoto, K. *Adv. Mater.* **2004**, *16*, 48.
- (87) Tronc, E.; Chanéac, C.; Jolivet, J. P.; Grenèche, J.-M. *J. Appl. Phys.* **2005**, *98*, 053901.
- (88) Ohkoshi, S.; Namai, A.; Sakurai, S. *J. Phys. Chem. C* **2009**, *113*, 11235.
- (89) Kurmoo, M.; Rehspringer, J.-L.; Hutlova, A.; D’Orléans, C.; Vilminot, S.; Estournès, C.; Niznansky, D. *Chem. Mater.* **2005**, *17*, 1106.
- (90) Rehspringer, J.-L.; Vilminot, S.; Niznansky, D.; Zaveta, K.; Estournès, C.; Kurmoo, M. *Hyperfine Interact.* **2005**, *166*, 475.
- (91) Gich, M.; Frontera, C.; Roig, A.; Fontcuberta, J.; Molins, E.; Bellido, N.; Simon, C.; Fleta, C. *Nanotechnology* **2006**, *17*, 687.
- (92) Ohkoshi, S.; Kuroki, S.; Sakurai, S.; Matsumoto, K.; Sato, K.; Sasaki, S. *Angew. Chem., Int. Ed.* **2007**, *46*, 8392.
- (93) Namai, A.; Sakurai, S.; Nakajima, M.; Suemoto, T.; Matsumoto, K.; Goto, M.; Sasaki, S.; Ohkoshi, S. *J. Am. Chem. Soc.* **2009**, *131*, 1170.
- (94) Han, Q.; Liu, Z. H.; Xu, Y. Y.; Chen, Z. Y.; Wang, T. M.; Zhang, H. *J. Phys. Chem. C* **2007**, *111*, 5034.
- (95) Wu, W.; Xiao, X. H.; Zhang, S. F.; Zhou, J. A.; Fan, L. X.; Ren, F.; Jiang, C. Z. *J. Phys. Chem. C* **2010**, *114*, 16092.
- (96) Wang, J. H.; Ma, Y. W.; Watanabe, K. *Chem. Mater.* **2008**, *20*, 20.
- (97) Hyeon, T.; Lee, S. S.; Park, J.; Chung, Y.; Bin, N. H. *J. Am. Chem. Soc.* **2001**, *123*, 12798.
- (98) Yin, M.; Willis, A.; Redl, F.; Turro, N. J.; O’Brien, S. P. *J. Mater. Res.* **2004**, *19*, 1208.
- (99) Bhalerao, G. M.; Sinha, A. K.; Srivastava, A. K. *J. Nanosci. Nanotechnol.* **2009**, *9*, 5502.
- (100) Rahman, M. M.; Venkataraman, A. *J. Therm. Anal. Calorim.* **2002**, *68*, 91.
- (101) Kluchova, K.; Zboril, R.; Tucek, J.; Pecova, M.; Zajoncova, L.; Safarik, I.; Mashlan, M.; Markova, I.; Jancik, D.; Sebela, M.; Bartonkova, H.; Belles, V.; Novak, P.; Petridis, D. *Biomaterials* **2009**, *30*, 2855.
- (102) Schimanke, G.; Martin, M. *Solid State Ionics* **2000**, *136*, 1235.
- (103) Zboril, R.; Machala, L.; Mashlan, M.; Hermanek, M.; Miglierini, M.; Fojtik, A. In *Proceedings of Second Seeheim Conference on Magnetism*;

- Ghafari, M.; Enz, T.; Hahn, H., Eds.; Wiley-VCH: Weinheim, Germany, 2004; p 3583.
- (104) Ninjabdar, T.; Yamamoto, S.; Takano, M. *Solid State Sci.* **2005**, *7*, 33.
- (105) Zhang, T. S.; Luo, H. M.; Zeng, H. M.; Zhang, R. F.; Shen, Y. S. *Sens. Actuators, A* **1996**, *32*, 181.
- (106) Kido, O.; Higashino, Y.; Kamitsuji, K.; Kurumada, M.; Sato, T.; Kimura, Y.; Suzuki, H.; Saito, Y.; Kaito, C. *J. Phys. Soc. Jpn.* **2004**, *73*, 2014.
- (107) Shebanova, O. N.; Lazor, P. *J. Raman Spectrosc.* **2003**, *34*, 845.
- (108) Helgason, O.; Grenache, J.-M.; Berry, F. J.; Mosselmans, F. *J. Phys.: Condens. Matter* **2003**, *15*, 2907.
- (109) Yen, F. S.; Chen, W. C.; Yang, J. M.; Hong, C. T. *Nano Lett.* **2002**, *2*, 245.
- (110) Ennas, G.; Marongiu, G.; Musinu, A.; Falqui, A.; Ballirano, P.; Caminiti, R. *J. Mater. Res.* **1999**, *14*, 1570.
- (111) Belin, T.; Millot, N.; Bovet, N.; Gailhanou, M. *J. Solid State Chem.* **2007**, *180*, 2377.
- (112) Navrotsky, A.; Mazeina, L.; Majzlan, J. *Science* **2008**, *319*, 1635.
- (113) Gnanaprakash, G.; Ayyappan, S.; Jayakumar, T.; Philip, J.; Raj, B. *Nanotechnology* **2006**, *17*, 5851.
- (114) Ye, X. S.; Lin, D. S.; Jiao, Z. K.; Zhang, L. D. *J. Phys. D: Appl. Phys.* **1998**, *31*, 2739.
- (115) Xu, X. B.; Ge, M. Y.; Wang, C.; Jiang, J. *Z. Appl. Phys. Lett.* **2009**, *95*, 183112.
- (116) Deka, S.; Joy, P. A. *J. Mater. Chem.* **2007**, *17*, 453.
- (117) Zhang, T. S.; Luo, H. M.; Zeng, H. M.; Zhang, R. F.; Shen, Y. S. *Sens. Actuators, B* **1996**, *32*, 181.
- (118) Zboril, R.; Bakandritsos, A.; Mashlan, M.; Tzitzios, V.; Dallas, P.; Trapalis, C.; Petridis, D. *Nanotechnology* **2008**, *19*, 095602.
- (119) Taboada, E.; Gich, M.; Roig, A. *ACS Nano* **2009**, *3*, 3377.
- (120) Barick, K. C.; Varaprasad, B. S. D. C. S.; Bahadur, D. *J. Non-Cryst. Solids* **2010**, *356*, 153.
- (121) Gich, M.; Roig, A.; Taboada, E.; Molins, E.; Bonafo, C.; Snoeck, E. *Faraday Discuss.* **2007**, *136*, 345.
- (122) Ding, Y.; Morber, J. R.; Snyder, R. L.; Wang, Z. L. *Adv. Funct. Mater.* **2007**, *17*, 1172.
- (123) Battisha, I. K.; Afify, H. H.; Hamada, I. M. *J. Magn. Magn. Mater.* **2005**, *292*, 440.
- (124) Ennas, G.; Musinu, A.; Piccaluga, G.; Zedda, D.; Gatteschi, D.; Sangregorio, C.; Stanger, J. L.; Concas, G.; Spano, G. *Chem. Mater.* **1998**, *10*, 495–502.
- (125) Jolivet, J. P.; Tronc, E.; Chaneac, C. C. R. *Geosci.* **2006**, *338*, 488.
- (126) Sartoratto, P. P. C.; Caiado, K. L.; Pedroza, R. C.; da Silva, S. W.; Moraes, P. C. *J. Alloys Compd.* **2007**, *434*, 650.
- (127) Zboril, R.; Mashlan, M.; Barcova, K.; Vujtek, M. *Hyperfine Interact.* **2002**, *139*, 597.
- (128) Barcova, K.; Mashlan, M.; Zboril, R.; Martinec, P.; Kula, P. *Czech. J. Phys.* **2001**, *51*, 749.
- (129) Barcova, K.; Mashlan, M.; Martinec, P. *Hyperfine Interact.* **2002**, *139*, 463.
- (130) Zboril, R.; Mashlan, M.; Papaefthymiou, V.; Hadjipanayis, G. *J. Radioanal. Nucl. Chem.* **2003**, *255*, 413.
- (131) Zboril, R.; Machala, L.; Mashlan, M.; Sharma, V. K. *Cryst. Growth Des.* **2004**, *4*, 1317.
- (132) Sivula, K.; Zboril, R.; Le Formal, F.; Robert, R.; Weidenkaff, A.; Tucek, J.; Frydrych, J.; Gratzel, M. *J. Am. Chem. Soc.* **2010**, *132*, 7436.
- (133) Pal, B.; Sharon, M. *Thin Solid Films* **2000**, *379*, 83.
- (134) Aronniemi, M.; Lahtinen, J.; Hautojarvi, P. *Surf. Interface Anal.* **2004**, *36*, 1004.
- (135) Kumar, A.; Singhal, A. *Nanotechnology* **2009**, *20*, 295606.
- (136) Lee, C. W.; Kim, S. G.; Lee, J. S. In *Science of Engineering Ceramics III*; Ohji, T., Sekino, T., Niijima, K., Eds.; Trans Tech Publications Inc.: Ueikon-Zürich, Switzerland, 2006; Vol. 317–318, p 219.
- (137) Lee, J. S.; Im, S. S.; Lee, C. W.; Yu, J. H.; Choa, Y. H.; Oh, S. T. *J. Nanoparticle Res.* **2004**, *6*, 627.
- (138) Ueyama, R.; Kurabayashi, K.; Itoh, N. *J. Ceram. Soc. Jpn.* **1996**, *104*, 949.
- (139) Liang, Y. Q.; van de Krol, R. *Chem. Phys. Lett.* **2009**, *479*, 86.
- (140) Ohkoshi, S.; Sakurai, S.; Jin, J.; Hashimoto, K. *J. Appl. Phys.* **2005**, *97*, 10K312.
- (141) Jin, J.; Hashimoto, K.; Ohkoshi, S. *J. Mater. Chem.* **2005**, *15*, 1067.
- (142) Ohkoshi, S.; Kuroki, S.; Sakurai, S.; Matsumoto, K.; Sato, K.; Sasaki, S. *Angew. Chem., Int. Ed.* **2007**, *46*, 8392.
- (143) Namai, A.; Sakurai, S.; Ohkoshi, S. *J. Appl. Phys.* **2009**, *105*, 07B516.
- (144) Sakurai, S.; Kuroki, S.; Tokoro, H.; Hashimoto, K.; Ohkoshi, S. *Adv. Funct. Mater.* **2007**, *17*, 2278.
- (145) Zboril, R.; Machala, L.; Mashlan, M.; Hermanek, M. In *Industrial Applications of the Mössbauer Effect: International Symposium on the Industrial Applications of the Mössbauer Effect Madrid (Spain), 4–8 October 2004, AIP Conference Proceedings*; Gracia, M., Marco, J. F., Plazaola, F., Eds.; American Institute of Physics: Melville, NY, 2005; Vol. 765, p 257.
- (146) Hermanek, M.; Zboril, R. *Chem. Mater.* **2008**, *20*, 5284.
- (147) Randrianantoandro, N.; Mercier, A. M.; Hervieu, M.; Grenache, J.-M. *Mater. Lett.* **2001**, *47*, 150.
- (148) Meillon, S.; Dammark, H.; Flavin, E.; Pascard, H. *Philos. Mag. Lett.* **1995**, *72*, 105.
- (149) Chernyshova, I. V.; Hochella, M. F.; Madden, A. S. *Phys. Chem. Chem. Phys.* **2007**, *9*, 1736.
- (150) Wilson, N. C.; Russo, S. P. *Phys. Rev. B* **2009**, *79*, 094113.
- (151) Kozhevnikov, A. V.; Lukoyano, A. V.; Anisimov, V. I.; Korotin, M. A. *J. Exp. Theor. Phys.* **2007**, *105*, 1035.
- (152) Clark, S. M.; Prilliman, S. G.; Erdonmez, C. K.; Alivisatos, A. P. *Nanotechnology* **2005**, *16*, 2813.
- (153) Kawakami, T.; Nasu, S.; Tsutsui, T.; Sasaki, T.; Yamada, T.; Endo, S.; Takano, M.; Katamoto, T. *J. Phys. Soc. Jpn.* **2003**, *72*, 2640.
- (154) Wang, Z. W.; Saxena, S. K. *Solid State Commun.* **2002**, *123*, 195.
- (155) Jiang, J. Z.; Olsen, J. S.; Gerward, L.; Mørup, S. *Europhys. Lett.* **1998**, *44*, 620.
- (156) Vaidya, S. N.; Karunakaran, C.; Aruna, S. T. *High Pressure Res.* **2001**, *21*, 79.
- (157) Zhao, J.; Guo, L.; Liu, J.; Yang, Y.; Che, R. Z.; Zhou, L. *Chin. Phys. Lett.* **2000**, *17*, 126.
- (158) Zhu, H.; Yang, D.; Zhu, L.; Yang, H.; Jin, D.; Yao, K. *J. Mater. Sci.* **2007**, *42*, 9205.
- (159) Lai, J.; Shafi, K. V. P. M.; Loos, K.; Ulman, A.; Lee, Y.; Vogt, T.; Estournès, C. *J. Am. Chem. Soc.* **2003**, *125*, 11470.
- (160) Ye, X. S.; Sha, J.; Song, H. Q.; Jiao, Z. K.; Lu, G. L.; Peng, Z. F.; Zhang, L. *Chin. Sci. Bull.* **1997**, *42*, 894.
- (161) Stefanescu, M.; Stefanescu, O.; Stoia, M.; Lazau, C. *J. Therm. Anal. Calorim.* **2007**, *88*, 27.
- (162) Ichiyanagi, Y.; Kimishima, Y. *J. Therm. Anal. Calorim.* **2002**, *69*, 919.
- (163) Varadwaj, K. S. K.; Panigrahi, M. K.; Ghose, J. *J. Solid State Chem.* **2004**, *177*, 4286.
- (164) Mendili, Y.; El; Bardeau, J.-F.; Randrianantoandro, N.; Gourbil, A.; Grenache, J.-M.; Mercier, A.-M.; Grasset, F. *J. Raman Spectrosc.* **2001**, *42*, 239.
- (165) Zhang, X. J.; Han, Q.; Dong, Z.; Xu, Y. Y.; Zhang, H. *J. Mater. Sci. Technol.* **2008**, *24*, 594.